AD-A064 394 AIR FORCE INST OF TECH WRIGHT-PATTERSON AFB OHIO SCH--ETC F/G 20/5
PHOTON STATISTICS IN TWO-MODE LASERS.(U)
DEC 78 B R ANDERSON

UNCLASSIFIED AFIT/GEP/PH/78-1 NL

1 OF 2
AD A064394

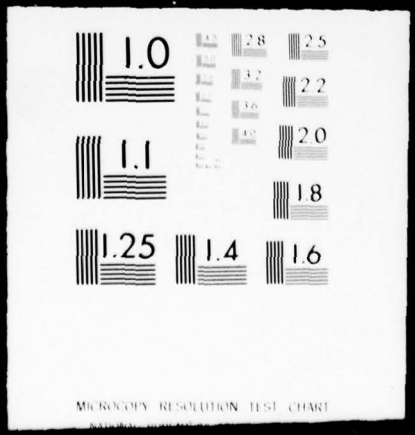

AFIT/GEP/PH/78-1

(1)

AD A064394

DDC FILE COPY

PHOTON STATISTICS IN TWO-MODE LASERS

THESIS

AFIT/GEP/PH/78-1 Bruce R. Anderson
Capt USAF

Approved for public release; distribution unlimited

AFIT/GEP/PH/78-1

(6) PHOTON STATISTICS IN TWO-MODE LASERS.

(9) Master's thesis,

THESIS

Presented to the Faculty of the School of Engineering

of the Air Force Institute of Technology

Air University

in Partial Fulfillment of the

Requirements for the Degree of

Master of Science

(12) 97 P

(14) AFIT/GEP/PH/78-1

by

(10) Bruce R. Anderson, B.S.

Capt USAF

Graduate Engineering Physics

(11) December 1978

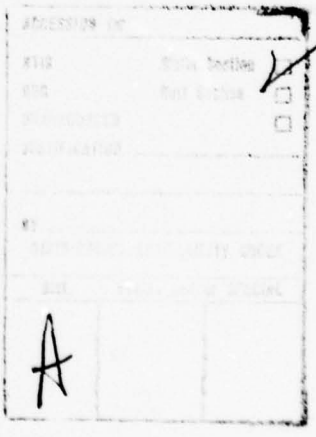

012 225

Acknowledgements

I would like to thank my advisor Dr. Donn Shankland for his assistance and inspiration throughout this study, especially in the suggested approach and development of equations. I would also like to thank Dr. Hugo Weichel for his helpful suggestions in the development of the background theory. Finally, I would like to thank my wife and family for their support and understanding.

Bruce R. Anderson

Contents

Contents

List of Figures

List of Figures (cont.)

List of Tables

List of Symbols

Symbol	
a, b, c, d	coefficients of linearized rate equations
a_1, a_2	gain coefficients ($a_i = g_{2i} - h_i$)
a_1', a_2'	effective gain coefficients
a_{n_1}	upward transition rate for n_1
$\underline{\underline{B}}$	general covariance tensor
BLCKDQ	subroutine used to solve the system of rate equations numerically
b_{n_1}	downward transition rate for n_1
C	coupling constant
c_{n_2}	upward transition rate for n_2
$\underline{c}_1$	first moment of the transition rate $w(\underline{y}, \underline{r})$
$\underline{\underline{c}}_2$	second moment of the transition rate $w(\underline{y}, \underline{r})$
d_{n_2}	downward transition rate for n_2
$\underline{\underline{E}}$	identity tensor
FCN	subroutine containing the rate equations
g_{11}, g_{22}	spontaneous emission terms
g_{21}, g_{22}	stimulated emission terms
h_1, h_2	cavity loss coefficients
I_1, I_2	dimensionless intensities of the electric fields in modes 1 and 2
K_1, K_2	coupling coefficients between the lasing mode and the lasing medium
l_1, l_2	equilibrium lines for modes 1 and 2
N_l	population density of lower lasing level
N_u	population density of upper lasing level
NMAX	plotting area dimension in (n_1, n_2) space
n_1, n_2	photon number densities for modes 1 and 2
n_1^o, n_2^o	photon number densities at equilibrium
n_1', n_2'	small density disturbance around equilibrium
n^k	kth moment of the photon distribution
$P(\underline{X}, t)$	probability distribution of $\underline{X}$
$P(\underline{x}, t)$	probability distribution of $\underline{x}$

Symbol	
$\underline{r}$	transition vector (always in terms of the extensive variable)
s_1, s_2	standard deviations
$W(\underline{X},\underline{r})$	transition rate for a jump from $\underline{X}$ by an amount $\underline{r}$
$w(\underline{x},\underline{r})$	transition rate for a jump from $\underline{x}$ by an amount $\underline{r}$/
$\underline{X}$	extensive macrovariable
XIN	time at which BLCKDQ begins
XOUT	time at which BLCKDQ provides solutions to the rate equations
$\underline{x}$	intensive macrovariable
Δx	small change in x
$\underline{Y}$	expected value of $\underline{x}$
$\underline{z}$	fluctuation of $\underline{x}$ about $\underline{y}$
α_{11}, α_{22}	saturation coefficients used in rate equations
α_{12}, α_{21}	coupling coefficients used in rate equations
α	linear gain coefficient
β	saturation coefficient
β_1, β_2	saturation coefficients
Θ_{12}, Θ_{21}	coupling coefficients
$\underline{\underline{\Lambda}}$	general inverse covariance tensor
$\underline{\underline{\lambda}}$	covariance tensor for $\underline{X}$
γ	loss coefficient
ρ_{12}	correlation coefficient
ρ_{nn}	diagonal elements of the field density matrix
$\underline{\underline{\sigma}}$	covariance tensor for $\underline{x}$
τ_c	photon cavity lifetime
Ω	size of the system
$\sim$	denotes transpose of a vector or tensor quantity

Abstract

The evolution of the first and second moments of the photon density distribution for a two-mode laser system was studied by proposing appropriate transition rate expressions and using the Kubo equations developed for a Chapman-Kolmogorov system. A numerical analysis technique was used in solving the rate equations and computer plots were generated for various combinations of laser parameter values. Anomalously large fluctuations, similar to those occurring in single-mode lasers, were observed during photon buildup of the modes. When only one mode was oscillating, a photon buildup in the non-lasing mode was seen to cause similar fluctuations in the lasing mode. In all cases, these fluctuations were accompanied by a strong linear relationship between the modes.

PHOTON STATISTICS IN TWO-MODE LASERS

I Introduction

Background

Since the development of the laser in 1960, the statistics for single-mode lasers have been studied extensively using both the semiclassical approach and the fully quantum-mechanical theory. Calculations have been made of the single-mode photon distributions below, at, and above threshold. Calculations have also been made of the time-behavior of the moments of the photon distribution as the laser operates away from equilibrium. These calculations have subsequently been verified by experiment.

The statistics for multimode lasers are not as well developed. Only the two-mode laser has been studied in any detail; and then, using only the semiclassical approach which neglects the particle or quantized nature of the light field in favor of a classical electric field. The fully quantum-mechanical treatment has just recently begun to be analyzed.

Purpose

The purpose of this work was to extend the study of two-mode lasers by investigating the photon distributions in equilibrium and the time behavior of the first and second moments of the distributions away from equilibrium for a two-mode laser. Of particular interest was the behavior of the system (for several pump levels and degrees of mode interaction) during buildup of photons from a photon vacuum and during transition from unstable to stable equilibrium. Transition from various

non-equilibrium points was also considered.

Approach

To study the behavior of the laser system, it was assumed that the system could be described by the Chapman-Kolmogorov master equation. Therefore, the resultant general evolution equations developed by Kubo were applicable. Transition rates which included terms to account for spontaneous and stimulated emission, as well as mode interaction and self-saturation, were proposed for the laser. These were then inserted into the general evolution equations, and rate equations for the first and second moments of the photon density distributions were obtained.

Appropriate values corresponding to various combinations of pump levels and degrees of mode coupling were chosen for the laser parameters. For each combination, the pump was considered constant while the coupling was assumed to take place through the mode population densities. The equilibrium points for each set of laser parameters were then obtained analytically from the rate equations and were classified using linear vibration theory to predict the behavior of the photon densities around each point.

To solve the moment rate equations dynamically and observe the laser system through transition, a computational scheme was developed which included a time-incremented numerical solution of the equations. Finally, using a series of initial photon densities with associated variances, this program was run for each combination of parameter values and several plots were obtained.

II Theory

Background

Just as there are two basic approaches to quantum mechanics, there are two main methods for deriving laser fluctuations fully quantum-mechanically. One method (associated more with the Schroedinger picture) utilizes a density operator to derive a "master equation". The other method (associated more with the Heisenberg picture) consists of "adding Langevin operators to the Heisenberg equation of the field operator and of the atomic operators" (Ref 9:273). The two methods are equivalent in that they solve the problem equally well. However, the master equation approach is more appropriate in that the resulting non-linear equations can be reduced to a form solvable by numerical methods, whereas the Langevin method requires analytical solutions which restrict its use to linear or linearized equations (Ref 9:273). Details of both methods can be found in the work of Sargent, Scully, and Lamb (Ref 11).

Single-Mode Theory. Using the master equation approach for single-mode lasers, the probabilities of n photons existing are determined by the diagonal elements ρ_{nn} of the associated field density matrix (Ref 11:284). Therefore, the equations of motion for these elements determine the flow of probability into and out of each n state:

$$\dot{\rho}_{nn}(t) = -\left[\alpha-\beta(n+1)\right](n+1)\,\rho_{nn}(t) + (\alpha-\beta n)n\,\rho_{n-1,n-1}(t) - \gamma n\,\rho_{nn}(t) + \gamma(n+1)\rho_{n+1,n+1}(t) \quad (1)$$

where α is the linear gain coefficient, γ is the loss coefficient,

β is the saturation coefficient, and the sign (positive or negative) of each term on the right-hand side indicates probability gains or losses, respectively, for the state n (Ref 10:2424). The photon distribution is then determined by solving these equations (Eqs (1)). It is important to note that the diagonal elements ρ_{nn} are coupled only to other diagonal elements. Therefore, to determine the photon statistics, the off-diagonal elements of the density matrix can be ignored.

In studying the behavior of any system, it is often of interest to consider the behavior of the moments of the distribution defined by

$$\langle n^k \rangle = \sum_{n=0}^{\infty} n^k p_n \qquad (2)$$

where p_n is synonymous with ρ_{nn} above. When Eq (1) is substituted into the time derivative of Eq (2), the result is a set of equations of motion for the moments of the photon distribution which can then be solved numerically to observe the behavior of the moments at as well as away from equilibrium. Of particular interest are the first and second moments ($k = 1$ and $k = 2$, respectively) since they can often be determined experimentally for comparison, whereas the distribution function cannot.

The behavior of these moments has been calculated from the initial condition that no photons exist to equilibrium conditions (Ref 10:2426-2427). The results for the expected value of the photon number (first moment) show an initial slow rise dominated by spontaneous emission, followed quickly by a rapid, almost linear, increase as the spontaneous emission is amplified by stimulated emission. However, as equilibrium is approached, the saturation effects of the laser begin to modify the system gain and the rate of increase of the average photon number approaches zero. The root mean squre deviation is determined by

combining the first and second moments:

$$S = \sqrt{\langle n^2 \rangle - \langle n \rangle^2} \tag{3}$$

This deviation initially tends to follow an exponential rise as for thermal (incoherent) light and exceeds the equilibrium value as not only the photon numbers, but also the fluctuations in photon numbers, are amplified. Then, as the system moves into the saturation region, amplification of already stimulated photons becomes predominant and the deviations diminish to their relatively small equilibrium values. It is important to note that when this problem was solved semiclassically, using Langevin forces to account for noise, similar results were obtained (Ref 9:262-263).

Two-Mode Theory. Unlike single-mode lasers, the fully quantum-mechanical treatment of multimode lasers has only very recently begun to be analyzed (Ref 8). Therefore, for these lasers the theory remains centered primarily around Lamb's paper (Ref 7) which gave the first comprehensive treatment of laser action. Following this semiclassical theory, the equations of motion for a two-mode laser system are

$$\dot{I}_1 = 2I_1(a_1 - \beta_1 I_1 - \theta_{12} I_2) \tag{4}$$

and

$$\dot{I}_2 = 2I_2(a_2 - \beta_2 I_2 - \theta_{21} I_1) \tag{5}$$

where I_1 and I_2 are the dimensionless intensities of the electric fields for the two modes, a_1 and a_2 are the gain coefficients, β_1 and β_2 are the self-saturation coefficients, and θ_{12} and θ_{21} are the cross-coupling coefficients. When these equations are integrated simultaneously for a range of initial intensities, the result is a set of phase

curves in the I_1-I_2 plane (Refs 7:A1441-A1442; and 11:125-127).

The possible equilibrium points are determined by setting $\dot{I}_1 = \dot{I}_2 = 0$ and solving (4) and (5) together. I_1 and/or I_2 equal to zero are obvious solutions, with single frequency solutions of

$$(I_1, I_2) = (0, a_2/\beta_2) \tag{6}$$

and

$$(I_1, I_2) = (a_1/\beta_1, 0) \tag{7}$$

For both modes to oscillate at equilibrium, the parenthesized expressions in (4) and (5) must be zero. Therefore,

$$\beta_1 I_1 + \theta_{12} I_2 = a_1 \tag{8}$$

and

$$\beta_2 I_2 + \theta_{21} I_1 = a_2 \tag{9}$$

which are linear expressions in I_1 and I_2 and have the solutions

$$I_1 = \frac{[a_1 - (\theta_{21}/\beta_2) a_2]/\beta_1}{1 - C} \tag{10}$$

$$I_2 = \frac{[a_2 - (\theta_{12}/\beta_1) a_1]/\beta_2}{1 - C} \tag{11}$$

where the coupling constant is defined as

$$C \equiv \frac{\theta_{12}\,\theta_{21}}{\beta_1\,\beta_2} \tag{12}$$

For this solution to be a physically realizeable point, both I_1 and I_2

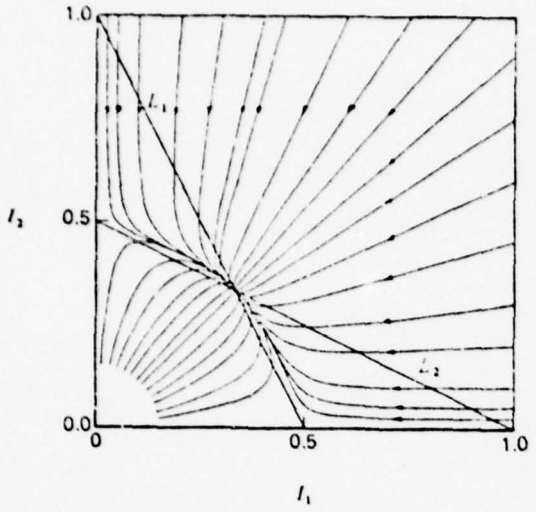

Figure 1. Phase curves showing the transient behavior of two mode oscillation. Lines L_1 and L_2 represent Eqs (8) and (9) with coefficients $a_1 = 1$, $a_2 = 1$, $\beta_1 = \beta_2 = 2$, and $\theta_{12} = \theta_{21} = 1$. (Ref 11:126)

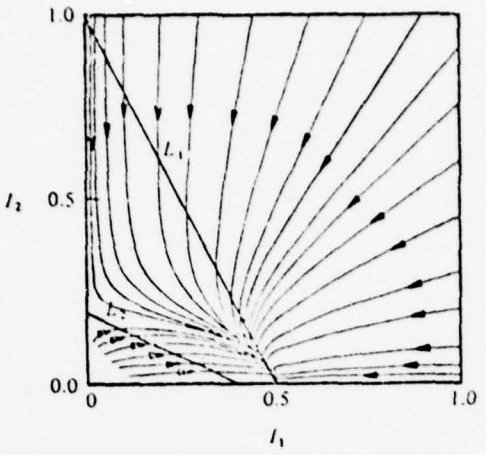

Figure 2. Diagram similar to Fig. 1, except the gain parameter for the second mode is now $a_2 = 0.4$, and mode 1 inhibits mode 2 at equilibrium. (Ref 11:125)

must be non-negative values. When $C < 1$, this occurs when both

$$a_1' = a_1 - (\theta_{21}/\beta_2)\, a_2 \qquad (13)$$

and

$$a_2' = a_2 - (\theta_{12}/\beta_1)\, a_1 \qquad (14)$$

are non-negative. See Fig. 1 (Ref 11:126). a_1' and a_2' are called the effective gains of their respective modes. If either effective gain is negative, then the associated mode will not oscillate and the laser will lapse into single-mode operation as shown in Fig. 2 (Ref 11:125) with mode intensities as defined by either (6) or (7), as appropriate. In this case, assuming both a_1 and a_2 are positive, the oscillating mode is said to inhibit oscillation in the other mode.

When $C>1$, the intersection of the two lines (8) and (9) is a physical point only when both a_1' and a_2' are non-positive; that is, when each mode tends to inhibit the other. In this case, the intersection point is an unstable equilibrium and, as with the inhibition of one mode, the system relaxes into single-mode operation. Now, however, both single-mode solutions defined by (6) and (7) are stable solutions and the point to which the system evolves depends on the initial conditions. See Fig. 3 (Ref 11:127).

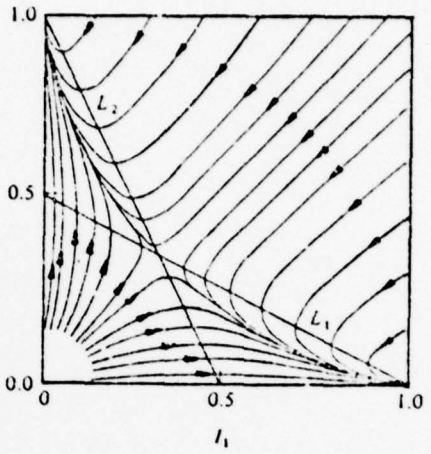

Figure 3. Phase curves showing the transient behavior of two-mode oscillation with coefficients $a_1 = a_2 = 1$, $\beta_1 = \beta_2 = 1$, and $\theta_{12} = \theta_{21} = 2$. (Ref 11:127)

When $C = 1$, lines (8) and (9) are parallel and Eqs (10) and (11) are indeterminate. In this instance, any combination of intensities on either mode equilibrium line (as defined by Eqs (8) and (9)) will be stable. Along these lines, the stability will be neutral with any deviations neither damped nor magnified. Deviations away from these lines, however, will decay in time, bringing the system back to the line.

As can be seen, the degree of coupling between modes, as expressed by the coupling constant C, is an important factor in determining the behavior of the system. The critical point is when $C = 1$. Therefore, three regions of coupling strength are defined:

$C < 1$ weak coupling (15a)

$C = 1$ neutral coupling (15b)

$C > 1$ strong coupling (15c)

where the degree of coupling applied to each region was determined by considering Eq (12) and the relationship of $\theta_{12}\theta_{21}$ to $\beta_1\beta_2$. Weak coupling implies that the cross-coupling coefficients, while they exist and affect the system, are not the dominant terms. Instead, the self-saturation coefficients are primarily responsible for limiting the growth of the system. Qualitatively, this is expressed as $\theta_{12}\theta_{21} < \beta_1\beta_2$ or $C < 1$. Conversely, strong coupling indicates that cross-coupling is the dominant effect, and is expressed as $\theta_{12}\theta_{21} > \beta_1\beta_2$. Neutral coupling, then, corresponds to neither effect dominant, or $\theta_{12}\theta_{21} = \beta_1\beta_2$.

Derivation of Moment-Rate Equations

General Evolution Equations. The two-mode laser (or more correctly, the two laser modes) can be considered as a system composed of many elementary units which interact with themselves and with the environment. As such, a set of macrovariables is defined:

$$\underline{X} = (X_1, X_2) \tag{16}$$

where X_1 and X_2 represent the photon numbers present in modes 1 and 2, respectively. It is assumed that $\underline{X}$ is a stochastic variable which follows a Markovian process as it evolves in time. Therefore, the master equation of the system is the Chapman-Kolmogorov equation, which may be written as

$$\frac{\partial}{\partial t} P(\underline{X},t) = -\int W(\underline{X},\underline{r}) P(\underline{X},t)\, d\underline{r} + \int W(\underline{X}-\underline{r},\underline{r}) P(\underline{X}-\underline{r},t)\, d\underline{r} \tag{17}$$

where $P(\underline{X},t)$ is the probability distribution of $\underline{X}$ (i.e., the probability that there exist X_1 photons in mode 1 and X_2 photons in mode 2) at time

t, and $W(\underline{X},\underline{r})$ is the transition rate for a jump from $\underline{X}$ by an amount $\underline{r}$. The evolution of variables governed by this equation has been studied extensively, beginning with the work of van Kampen (Ref 16) and continued by Kubo (Refs 4; 5; and 6) and Haken (Ref 3). Therefore, the resulting evolution equations for the system are just listed here:

$$\dot{\underline{y}}(t) = \underline{c}_1(\underline{y},t) \tag{18}$$

and

$$\dot{\underline{\underline{\sigma}}}(t) = \frac{1}{\Omega}\underline{\underline{c}}_2(\underline{y},t) + \underline{\underline{\sigma}}\,\nabla_y \underline{\tilde{c}}_1(\underline{y},t) + \overline{\left(\nabla_y \underline{\tilde{c}}_1(\underline{y},t)\right)}\,\underline{\underline{\sigma}} \tag{19}$$

where Ω is the size of the system, $\underline{y}(t)$ is the expected value of the normalized intensive macrovariable (representing the photon densities) of the system, $\underline{x}(t) = \underline{X}/\Omega$, and $\underline{\underline{\sigma}}(t)$ is the covariance tensor for $\underline{x}$. The variables $\underline{c}_1$ and $\underline{\underline{c}}_2$, as defined by

$$\underline{c}_1(\underline{y},t) = \int d\underline{r}\, \omega(\underline{y},\underline{r})\,\underline{\tilde{r}} \tag{20}$$

$$\underline{\underline{c}}_2(\underline{y},t) = \int d\underline{r}\, \omega(\underline{y},\underline{r})\,\underline{r}\,\underline{\tilde{r}} \tag{21}$$

are the first and second moments of $w(\underline{y},\underline{r})$, the transition rate for the intensive variable $\underline{x}$:

$$\omega(\underline{y},\underline{r}) = \omega(\underline{x},\underline{r}) = W(\underline{X},\underline{r})/\Omega \tag{22}$$

A derivation of Eqs (18) and (19), starting from (17) and parallelling the single variable derivation of Kubo (Ref 5), is included in Appendix A.

A general analysis of Eqs (18) and (19) predicts some interesting behavior on the part of the laser system. First, the expected values of the photon number densities follow deterministic paths. For a given set of laser operating conditions, the path to equilibrium is determined solely by the initial photon densities. For a non-linear relaxation, the fluctuations generally exhibit unusual behavior as the system moves toward equilibrium. This effect becomes very pronounced when the system moves from the vicinity of an unstable equilibrium toward a stable equilibrium. Around each point, both the photon number densities and their fluctuations grow or decay exponentially, depending on the stability of the point. In between, the fluctuations grow anomalously large, peaking about half-way to the final equilibrium. (Refs 6:78-79; and 4:6-8) This enhanced fluctuation is predicted for and has been observed in single-mode lasers (Ref 2). It has also been predicted for two-mode lasers by Arecchi and Ricca in a paper which used a generalized version of the Volterra-Wiener functional technique to study multimode laser action (Ref 1).

Transition Rates. To make the evolution equations (18) and (19) specific to the two-mode laser problem requires the proper specification of the transition rates $w(\underline{y},\underline{r})$. It is important to note that the size of the transition, $\underline{r}$, is in terms of the extensive variable $\underline{X}$ or the total number of photons, whereas the dependence on the state of the system is in terms of the intensive variable $\underline{x}$ or the photon density.

The basic problem is depicted in Fig. 4 for a system in the state $\underline{x}=(n_1,n_2)$. a_{n_1} and b_{n_1} are the upward and downward transition rates,

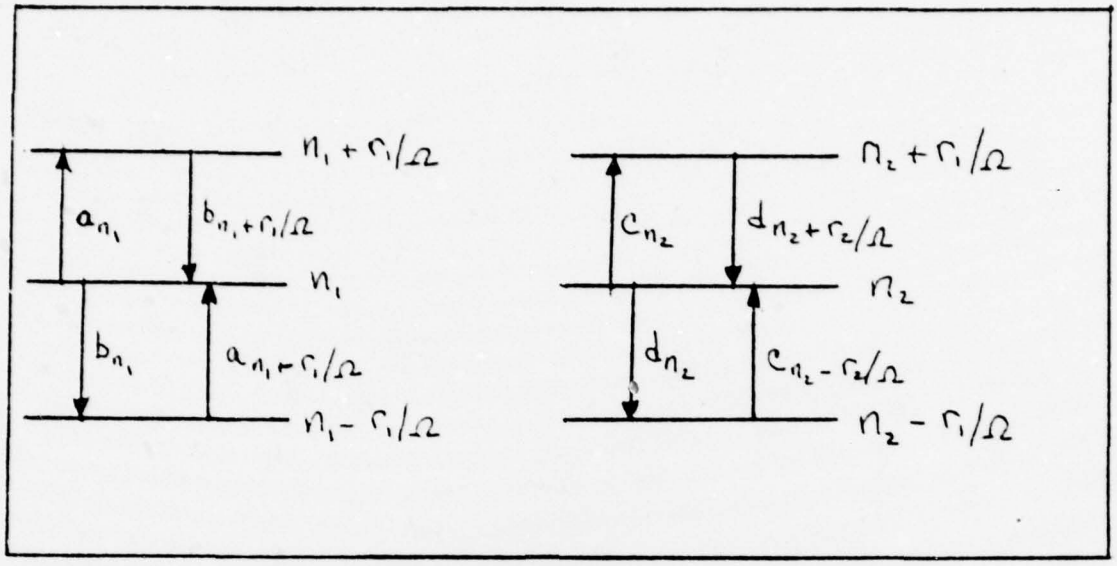

Figure 4. Transition rates associated with a laser system in the internal state $\underline{x} = (n_1, n_2)$. Upward transitions (↑) correspond to photon emissions while downward transitions (↓) signify photon losses.

respectively, for x_1 to make a jump r_1/Ω , and c_{n_2} and d_{n_2} are corresponding terms for x_2. It is assumed that photons are added to or deleted from the system one at a time. Therefore, the only non-zero values for r_1 and r_2 with associated non-zero rates are 1 and -1. Furthermore, even for these values, the associated rates for one mode will be non-zero only if $r_i = 0$ for the other mode. Therefore, there are only four events with non-zero associated transition rates: X_1 increases by one, $\underline{r} = (1,0)$; X_1 decreases by one, $\underline{r} = (-1,0)$; X_2 increases by one, $\underline{r} = (0,1)$; and X_2 decreases by one, $\underline{r} = (0,-1)$. Based on this and on Fig. 4, the transition rates for $\underline{x} = (n_1, n_2)$ can be written as

$$w(\underline{x},\underline{r}) = \begin{cases} a_{n_1}, & \underline{r} = (1,0) \\ b_{n_1}, & \underline{r} = (-1,0) \\ c_{n_2}, & \underline{r} = (0,1) \\ d_{n_2}, & \underline{r} = (0,-1) \end{cases} \qquad (23)$$

These rates are also valid for $w(\underline{y},\underline{r})$ since $\underline{y}(t)$ is just the expected value of $\underline{x}$.

How, then, should a_{n_1}, b_{n_1}, c_{n_2}, and d_{n_2} be characterized? b_{n_1} and d_{n_2} essentially are the loss terms of the system, including internal cavity losses as well as the amount coupled out of the system. Therefore, they can be expressed as

$$b_{n_1} = h_1 n_1 \tag{24}$$

and

$$d_{n_2} = h_2 n_2 \tag{25}$$

where h_1 and h_2 are determined by the cavity lifetime for a photon in modes 1 and 2, respectively (Ref 12:413). a_{n_1} and c_{n_2}, representing the gain of each mode of the system, are somewhat more complicated. Each gain expression must include terms to account for both stimulated and spontaneous emission as well as for self-saturation and cross-coupling. The self-saturation occurs because there is only a finite pump which excites a finite number of atoms or molecules which may then be stimulated to contribute to the system of photons. Cross-coupling occurs when both modes have to compete for some of the same atoms or molecules.

The expression chosen which meets these requirements for a_{n_1} is

$$a_{n_1} = \frac{g_{11} + g_{21} n_1}{1 + \alpha_{11} n_1 + \alpha_{12} n_2} \tag{26}$$

where g_{11} and g_{21} are factors accounting for spontaneous and stimulated emission, respectively, and α_{11} and α_{12} account for self-saturation and cross-coupling, respectively. A similar expression for c_{n_2} is

$$c_{n_2} = \frac{g_{12} + g_{22} n_2}{1 + \alpha_{21} n_1 + \alpha_{22} n_2} \tag{27}$$

with g_{12}, g_{22}, α_{21} and α_{22} having the same meaning for mode 2 as g_{11}, g_{21}, α_{12} and α_{22} do for mode 1. It is important to note that with these expressions the transition rates will always be non-negative. The validity of these choices will be demonstrated in a later section.

Laser Rate Equations. When the transition rates (Eqs (24)-(27)) are inserted into the evolution equations (18) and (19), the resultant equations are the desired laser rate equations for the first and second moments of the photon density distributions. For ease of manipulation, the evolution equations will be handled in their component form. Therefore, Eq (18) becomes

$$\dot{y}_j(t) = c_{1j}(\underline{y}) \tag{28}$$

and Eq (19) is written as

$$\dot{\sigma}_{jk}(t) = \frac{1}{\Omega} c_{2jk} + \sum_l \left(\sigma_{jl} \frac{\partial c_{1k}}{\partial y_l} + \frac{\partial c_{1j}}{\partial y_l} \sigma_{lk} \right) \tag{29}$$

where now $\underline{c}_1(\underline{y})$ and $\underline{\underline{c}}_2(\underline{y})$ are expressed as

$$c_{1j}(\underline{y}) = \int dr\, r_j\, \omega(\underline{y}, \underline{r}) \tag{30}$$

and

$$c_{2jk}(\underline{y}) = \int dr\, r_j r_k\, \omega(\underline{y}, \underline{r}) \tag{31}$$

Dealing first with Eq (30), Eqs (24)-(27) are appropriately inserted

into Eq (30) as determined by Eqs (23). The resulting components of $\underline{c}_1(\underline{y})$ are

$$c_{11}(\underline{y}) = \int dr\, r_1 \omega(\underline{y}, \underline{r})$$

$$= a_{n_1} + (-1) b_{n_1}$$

$$= \frac{g_{11} + g_{21} n_1}{1 + \alpha_{11} n_1 + \alpha_{12} n_2} - h_1 n_1 \qquad (32)$$

and

$$c_{12}(\underline{y}) = \int dr\, r_2 \omega(\underline{y}, \underline{r})$$

$$= c_{n_2} + (-1) d_{n_2}$$

$$= \frac{g_{12} + g_{22} n_2}{1 + \alpha_{21} n_1 + \alpha_{22} n_2} - h_2 n_2 \qquad (33)$$

Similarly, the diagonal elements of $\underline{\underline{c}}_2(\underline{y})$ are found from Eq (31) to be

$$c_{2_{11}} = \frac{g_{11} + g_{21} n_1}{1 + \alpha_{11} n_1 + \alpha_{12} n_2} + h_1 n_1 \qquad (34)$$

and

$$c_{2_{22}} = \frac{g_{12} + g_{22} n_2}{1 + \alpha_{21} n_1 + \alpha_{22} n_2} + h_2 n_2 \qquad (35)$$

Since mutually exclusive events were assumed, r_j or r_k must equal zero whenever $j \neq k$. Therefore, the off-diagonal elements of $\underline{\underline{c}}_2$ are both zero.

To complete the development of the rate equations, the partial derivatives of (32) and (33) with respect to y_1 and y_2 must be determined. In doing this, as throughout this development, it should be pointed out that n_1 and n_2 are defined as synonymous with y_1 and y_2, respectively. When this is done and Eqs (32)-(35) are inserted into Eqs (28) and (29) as appropriate, the rate equations for the first and second moments of the photon density distributions become

$$\dot{n}_1 = \frac{g_{11} + g_{21} n_1}{1 + \alpha_{11} n_1 + \alpha_{12} n_2} - h_1 n_1 \tag{36}$$

$$\dot{n}_2 = \frac{g_{12} + g_{22} n_2}{1 + \alpha_{21} n_1 + \alpha_{22} n_2} - h_2 n_2 \tag{37}$$

$$\dot{\sigma}_{11} = 2\sigma_{11}\left[\frac{g_{21} - g_{11}\alpha_{11} + g_{21}\alpha_{12} n_2}{(1 + \alpha_{11} n_1 + \alpha_{12} n_2)^2} - h_1\right] - 2\sigma_{12}\left[\frac{\alpha_{12}(g_{11} + g_{21} n_1)}{(1 + \alpha_{11} n_1 + \alpha_{12} n_2)^2}\right] + \frac{1}{\Omega}\left(\frac{g_{11} + g_{21} n_1}{1 + \alpha_{11} n_1 + \alpha_{12} n_2} + h_1 n_1\right) \tag{38}$$

$$\dot{\sigma}_{22} = 2\sigma_{22}\left[\frac{g_{22} - g_{12}\alpha_{22} + g_{22}\alpha_{21} n_1}{(1 + \alpha_{21} n_1 + \alpha_{22} n_2)^2} - h_2\right] - 2\sigma_{12}\left[\frac{\alpha_{21}(g_{12} + g_{22} n_2)}{(1 + \alpha_{21} n_1 + \alpha_{22} n_2)^2}\right] + \frac{1}{\Omega}\left(\frac{g_{12} + g_{22} n_2}{1 + \alpha_{21} n_1 + \alpha_{22} n_2} + h_2 n_2\right) \tag{39}$$

and

$$\dot{\sigma}_{12} = -\sigma_{11}\left[\frac{\alpha_{21}\left(g_{12}+g_{22}n_2\right)}{\left(1+\alpha_{21}n_1+\alpha_{22}n_2\right)^2}\right] - \sigma_{22}\left[\frac{\alpha_{12}\left(g_{11}+g_{21}n_1\right)}{\left(1+\alpha_{11}n_1+\alpha_{12}n_2\right)^2}\right]$$

$$+\sigma_{12}\left[\frac{g_{21}-g_{11}\alpha_{11}+g_{21}\alpha_{12}n_2}{\left(1+\alpha_{11}n_1+\alpha_{12}n_2\right)^2}+\frac{g_{22}-g_{12}\alpha_{22}+g_{22}\alpha_{21}n_1}{\left(1+\alpha_{21}n_1+\alpha_{22}n_2\right)^2}-h_1-h_2\right] \quad (40)$$

There is actually a sixth rate equation, for σ_{21}, but it is identical in form to (40). Also, the equality of σ_{12} and σ_{21} due to the symmetry of the covariance matrix is used to combine terms in Eqs (38), (39), and (40). Therefore, only the five equations (36)-(40) need be solved simultaneously to determine the behavior of the laser system.

Equilibrium Analysis of Moment Equations

As stated previously, the purpose of this study was to determine the behavior of a two-mode laser system as it transitioned from non-equilibria to equilibrium. This was the reason for developing the laser rate equations and solving them dynamically. However, before applying numerical methods to these equations to follow the system through its transition, a basic understanding of the system can be gained by determining analytically the positions of all equilibria, both stable and unstable, and the behavior of the system around each of these points. Of particular interest is the first-moment equilibria, since these values for n_1 and n_2 are necessary to do any equilibrium analysis on the variances. Therefore, the photon rate equations (36) and (37) are considered first, followed by a brief discussion of the variance rate equations (38), (39), and (40) in equilibrium.

First-Moment Equations. Recalling the first-moment or photon

density rate equations (36) and (37), equilibria will occur when both $\dot{n}_1$ and $\dot{n}_2$ are zero. These are also referred to as singular points of the system. The point $n_1 = n_2 = 0$ can only be a solution if $g_{11} = g_{12} = 0$; but this corresponds to zero noise or spontaneous emission in the system, which is an unrealizeable situation. In fact, neither n_1 nor n_2 equal tp zero can be a solution for finite values of n. Therefore, there is some combination of non-zero (n_1, n_2) for which equilibrium will exist.

As a first approximation, assume n_1 and $n_2 \gg 1$, $g_{11} = g_{21}$, and $g_{12} = g_{22}$. Then Eqs (36) and (37), set to equilibrium, become

$$\dot{n}_1 = 0 = \left[g_{21} / \left(1 + \alpha_{11} n_1 + \alpha_{12} n_2 \right) - h_1 \right] n_1 \qquad (41)$$

and

$$\dot{n}_2 = 0 = \left[g_{22} / \left(1 + \alpha_{21} n_1 + \alpha_{22} n_2 \right) - h_2 \right] n_2 \qquad (42)$$

Since only non-zero values of n_1 and n_2 are of interest, the bracketed quantities in (41) and (42) are set to zero and examined. After re-arranging, the resultant equations are

$$\alpha_{11} n_1 + \alpha_{12} n_2 = \frac{g_{21}}{h_1} - 1 \qquad (43)$$

and

$$\alpha_{21} n_1 + \alpha_{22} n_2 = \frac{g_{22}}{h_2} - 1 \qquad (44)$$

These are just two straight lines (call them l_1 and l_2, respectively) in (n_1, n_2) space with n_1- and n_2- intercepts of

$$\frac{1}{\alpha_{11}}\left(\frac{g_{21}}{h_1}-1\right) \quad \text{and} \quad \frac{1}{\alpha_{12}}\left(\frac{g_{21}}{h_1}-1\right) \tag{45}$$

for l_1, and

$$\frac{1}{\alpha_{21}}\left(\frac{g_{22}}{h_2}-1\right) \quad \text{and} \quad \frac{1}{\alpha_{22}}\left(\frac{g_{22}}{h_2}-1\right) \tag{46}$$

for l_2.

Within the limits of the original assumption ($n_1, n_2 \gg 1$), the point of intersection of these two lines is the location of *one* equilibrium or singular point. To find this point of intersection, equations (43) and (44) are solved simultaneously. This results in

$$n_1 = \frac{\frac{1}{h_1\alpha_{11}}\left(g_{21}-h_1\right) - \frac{\alpha_{12}}{\alpha_{11}}\frac{1}{h_2\alpha_{22}}\left(g_{22}-h_2\right)}{1-\frac{\alpha_{21}\alpha_{12}}{\alpha_{11}\alpha_{22}}} \tag{47}$$

and

$$n_2 = \frac{\frac{1}{h_2\alpha_{22}}\left(g_{22}-h_2\right) - \frac{\alpha_{21}}{\alpha_{22}}\frac{1}{h_1\alpha_{11}}\left(g_{21}-h_1\right)}{1-\frac{\alpha_{21}\alpha_{12}}{\alpha_{11}\alpha_{22}}} \tag{48}$$

Now, if the following substitutions are made,

$$g_{21}-h_1 = a_1 \qquad g_{22}-h_2 = a_2 \tag{49a}$$

$$h_1\alpha_{11} = \beta_1 \qquad h_2\alpha_{22} = \beta_2 \tag{49b}$$

$$h_1 \alpha_{12} = \theta_{12} \qquad h_2 \alpha_{21} = \theta_{21} \tag{49c}$$

equations (47) and (48) become

$$n_1 = \frac{(a_1 - (\theta_{12}/\beta_2)\, a_2)/\beta_1}{1 - C} \tag{50}$$

and

$$n_2 = \frac{(a_2 - (\theta_{21}/\beta_1)\, a_1)/\beta_2}{1 - C} \tag{51}$$

where

$$C = \frac{\alpha_{12}\,\alpha_{21}}{\alpha_{11}\,\alpha_{22}} = \frac{\theta_{12}\,\theta_{21}}{\beta_1\,\beta_2} \tag{52}$$

is a measure of the degree of coupling, as previously discussed. Comparing this to the semiclassical development of Lamb presented earlier, it is seen that Eqs (50) and (51) are essentially identical to Eqs (10) and (11) with the normalized intensities I_1 and I_2 replaced by their quantum equivalent, the photon number densities. Furthermore, when Eqs (41) and (42) are expressed as single fractions (with non-zero denominators), they can be reduced to

$$\dot{n}_1 = 0 = n_1 \left[(g_{21} - h_1) - h_1 \alpha_{11} n_1 - h_1 \alpha_{12} n_2 \right] \tag{53}$$

and

$$\dot{n}_2 = 0 = n_2 \left[(g_{22} - h_2) - h_2 \alpha_{22} n_2 - h_2 \alpha_{21} n_1 \right] \tag{54}$$

which are equivalent to Lamb's equations of motion for I_1 and I_2, Eqs (4) and (5), at equilibrium. Therefore, in the limits of equilibrium and of large n (or zero noise), the chosen transition rates a_{n_1}, b_{n_1}, c_{n_2}, and d_{n_2} are valid, and the semiclassical equilibrium analysis done by Lamb can be applied.

When the spontaneous emission terms g_{11} and g_{12} are not assumed away, the singularities for the system are determined by setting Eqs (36) and (37) to zero and solving simultaneously. Solving Eq (36) for n_2 and substituting the obtained expression into (37), the result is the fourth order equation

$$h_1^2 h_2 \alpha_{11}(\alpha_{12}\alpha_{21} - \alpha_{11}\alpha_{22}) n_1^4 + h_1\left[h_2(g_{21}-h_1)(2\alpha_{11}\alpha_{22} - \alpha_{12}\alpha_{21}) - h_1\alpha_{11}\alpha_{12}(g_{22}-h_2)\right] n_1^3 + \left[h_1\alpha_{12}(g_{12}h_1\alpha_{12} + (g_{22}-h_2)(g_{21}-h_1) - h_2\alpha_{21}g_{11}) + h_2\alpha_{22}(2g_{11}h_1\alpha_1 - (g_{21}-h_1)^2)\right] n_1^2 + \left[h_1 g_{11}\alpha_{12}(g_{22}-h_2) - 2g_{11}h_2\alpha_{22}(g_{21}-h_1)\right] n_1 - h_2\alpha_{22}g_{11}^2 = 0 \qquad (55)$$

This is then solved using basic algebraic techniques (Ref 14:107) and, depending on the coefficients, generally results in four singular points for the system.

Characterization of Singular Points. The behavior of the system around a given singularity is determined by considering a small disturbance around that point. Based on this behavior, the singularity can then be classified into one of six basic types, as shown in Fig. 5.

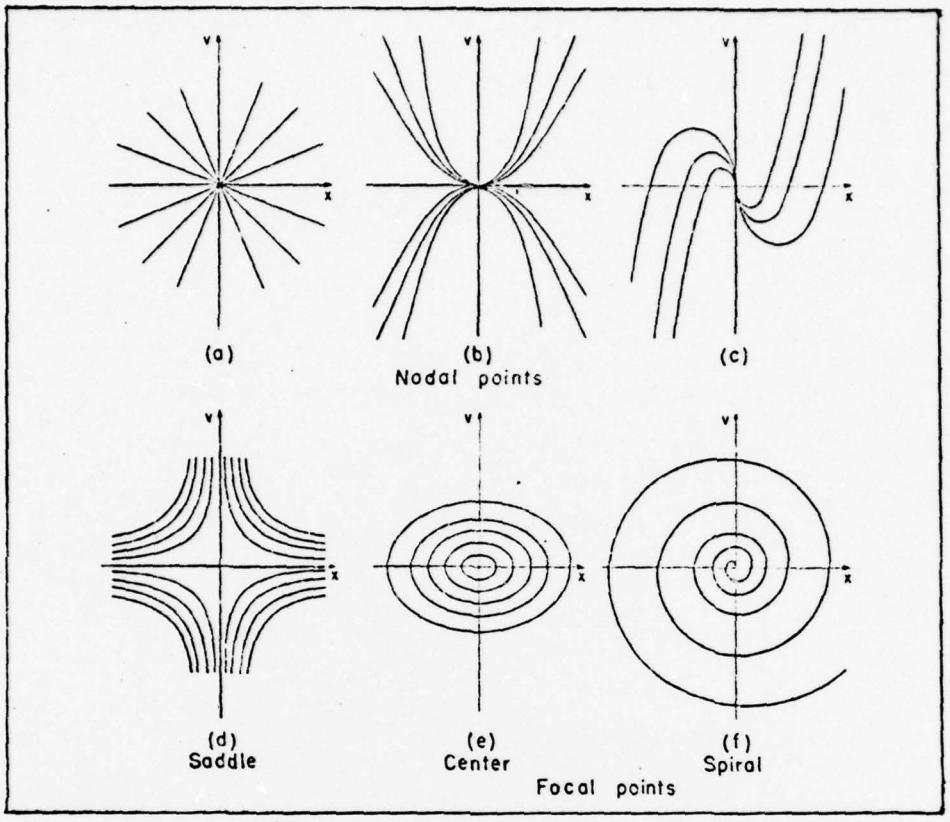

Figure 5. Types of Singular Points (Ref 15:39)

Letting $n_1 = n_1^\circ + n_1'$ and $n_2 = n_2^\circ + n_2'$ (where n_1° and n_2° are the singular point values) and inserting these into Eqs (36) and (37), the resulting linearized forms of the photon rate equations are

$$\dot{n}_1 = \frac{-h_1 \alpha_{12} n_1^\circ n_2' + (g_{21} - h_1 - 2h_1 \alpha_{11} n_1^\circ - h_1 \alpha_{12} n_2^\circ) n_1'}{1 + \alpha_{11} n_1^\circ + \alpha_{12} n_2^\circ} \quad (56)$$

and

$$\dot{n}_2 = \frac{(g_{22} - h_2 - 2h_2 \alpha_{22} n_2^\circ - h_2 \alpha_{21} n_1^\circ) n_2' - h_2 \alpha_{21} n_2^\circ n_1'}{1 + \alpha_{21} n_1^\circ + \alpha_{22} n_2^\circ} \quad (57)$$

For a complete development of Eqs (56) and (57) see Appendix B. These

equations can be combined in the form

$$\frac{dn_1'}{dn_2'} = \frac{an_2' + bn_1'}{cn_2' + dn_1'} \tag{58}$$

where

$$a = -h_1\alpha_{12}n_1^\circ \Big/ \left(1 + \alpha_{11}n_1^\circ + \alpha_{12}n_2^\circ\right) \tag{59a}$$

$$b = \left(g_{21} - h_1 - 2h_1\alpha_{11}n_1^\circ - h_1\alpha_{12}n_2^\circ\right) \Big/ \left(1 + \alpha_{11}n_1^\circ + \alpha_{12}n_2^\circ\right) \tag{59b}$$

$$c = \left(g_{22} - h_2 - 2h_2\alpha_{22}n_2^\circ - h_2\alpha_{21}n_1^\circ\right) \Big/ \left(1 + \alpha_{21}n_1^\circ + \alpha_{22}n_2^\circ\right) \tag{59c}$$

and

$$d = -h_2\alpha_{21}n_2^\circ \Big/ \left(1 + \alpha_{21}n_1^\circ + \alpha_{22}n_2^\circ\right) \tag{59d}$$

The type of singularity can then be determined by a series of expressions involving these coefficients. These expressions, and their relationships to the types of singular points as shown in Fig. 5, are as follows (Ref 15:44):

I. $(b-c)^2 + 4ad > 0$

- $ad - bc < 0$ — Node (Fig. 5a, 5b)
- $ad - bc > 0$ — Saddle (Fig. 5d)

II. $(b-c)^2 + 4ad < 0$

- $b + c = 0$ — Center (Fig. 5e)
- $b + c \neq 0$ — Spiral (Fig. 5f)

III. $(b-c)^2 + 4ad = 0$ — Node (Fig. 5c)

Also, a node or spiral is unstable or stable depending on whether $b + c$ is positive or negative, respectively.

Second-Moment Equations. Knowing the equilibrium values for the photon densities, the variance rate equations (38), (39), and (40) can be set to equilibrium and solved simultaneously. The zero of $\dot{\sigma}_{11}$ in Eq (38) represents a plane parallel to the σ_{22} axis in (σ_{11} , σ_{22} , σ_{12}) space. Similarly, Eq (39) represents a plane parallel to the σ_{11} axis, whereas Eq (40) is the equation for a straight line. Therefore, for a given singular point (n_1, n_2), there will be at most a single equilibrium point for the variances. Eqs (38) and (39) are solved for σ_{11} and σ_{22}, respectively, to get

$$\sigma_{11} = \frac{-(2B\sigma_{12} + C)}{2A} \tag{60}$$

and

$$\sigma_{22} = \frac{-(2E\sigma_{12} + C)}{2D} \tag{61}$$

where

$$A = (g_{21} - g_{11}\alpha_{11} + g_{21}\alpha_{12}n_2)(1 + \alpha_{11}n_1 + \alpha_{12}n_2)^{-2} - h_1 \tag{62a}$$

$$B = -\alpha_{12}(g_{11} + g_{21}n_1)(1 + \alpha_{11}n_1 + \alpha_{12}n_2)^{-2} \tag{62b}$$

$$C = \frac{1}{\Omega}\left[(g_{11} + g_{21}n_1)(1 + \alpha_{11}n_1 + \alpha_{12}n_2)^{-1} + h_1 n_1\right] \tag{62c}$$

$$D = (g_{22} - g_{12}\alpha_{22} + g_{22}\alpha_{21}n_1)(1 + \alpha_{21}n_1 + \alpha_{22}n_2)^{-2} - h_2 \tag{62d}$$

$$E = -\alpha_{21}(g_{12} + g_{22}n_2)(1 + \alpha_{21}n_1 + \alpha_{22}n_2)^{-2} \tag{62e}$$

and

$$F = \frac{1}{\Omega}\left[\left(g_{12} + g_{22}n_2\right)\left(1 + \alpha_{21}n_1 + \alpha_{22}n_2\right)^{-1} + h_2 n_2\right] \qquad (62f)$$

Eqs (60) and (61) are then inserted into Eq (40) and the resulting expression for σ_{12} is

$$\sigma_{12} = \frac{CED + ABF}{2\left[(A+D)(AD-EB)\right]} \qquad (63)$$

This value is then used in Eqs (60) and (61) to obtain corresponding values of σ_{11} and σ_{22}, respectively.

III Approach

Computational Scheme

In studying the behavior of the laser system using the laser rate equations (36)-(40), several steps were accomplished. The first of these was the development of a computer program which included the selection of a numerical analysis scheme capable of solving the system of rate equations (36)-(40) in arbitrary time increments. The routine chosen for this most important procedure is a FORTRAN IV subroutine called BLCKDQ (Ref 13). It uses a predictor-corrector formula of 8th order with user specified tolerances, which were set to 10^{-15} because of initial rapid changes in the moments. Time-incremented solutions are possible because BLCKDQ solves the system of equations at a user specified time (XOUT), given appropriate initial values at some prior user specified time (XIN). Therefore, the system is incremented to equilibrium by calling BLCKDQ within a loop where the "initial" values are set equal to the solutions from the previous time step, XIN is set equal to the previous XOUT, and XOUT is incremented by some predetermined amount. Built around this loop, the remainder of the program was then developed to solve the rate equations to equilibrium for a series of initial value points and to store for plotting all sets of solutions belonging to a given set of laser parameters. The laser rate equations are contained in a user supplied subroutine FCN which is called by BLCKDQ.

Selection of Values for Laser Parameters

The second step in making the rate equations solvable was to determine appropriate values for the various laser parameters (g_{ij}, α_i, h_i) for the desired combinatims of pump levels and degrees of coupling.

To do this, several assumptions were made. First, it was assumed that the cavity losses, the self-saturation, and the cross-coupling were the same for both modes. That is

$$h_1 = h_2 \tag{64a}$$

$$\alpha_{11} = \alpha_{22} \tag{64b}$$

$$\alpha_{12} = \alpha_{21} \tag{64c}$$

Comparing Siegman's photon rate equation (Ref 12:418) to Eqs (36) and (37), and noting that Siegman has no saturation or coupling terms, the following equivalences can be made:

$$g_{21} = K_1 (N_u - N_l) \tag{65a}$$

$$g_{22} = K_2 (N_u - N_l) \tag{65b}$$

$$g_{11} = K_1 N_u \tag{65c}$$

$$g_{12} = K_2 N_u \tag{65d}$$

where N_u and N_1 are population densities of the upper and lower lasing levels and K_1 and K_2 are coupling coefficients between the lasing modes and the lasing medium. It is assumed that the lower lasing level depopulates essentially instantaneously ($N_1 \approx 0$) and the upper lasing level is maintained constant. Therefore, $g_{11} = g_{21}$ = constant and $g_{12} = g_{22}$ = constant.

To select a value for h, the following relationship is noted (Ref 12:418):

$$h = 1/\tau_c \tag{66}$$

where τ_c is the photon cavity lifetime. A representative value for τ_c is 10^{-8} sec. Therefore

$$h = h_1 = h_2 = 10^8 \tag{67}$$

is used for all combinations of g_{ij} and α_{ij}. The saturation and coupling coefficients are somewhat more elusive. To get an idea of at least an order of magnitude, the expressions (49) were recalled and compared with values for β_i and θ_{ij} used by Lamb (Ref 11:121). Therefore, for each type of coupling (as determined by (6) and (52)), the following values were chosen:

$$\text{weak coupling } (C<1): \quad \alpha_{11} = \alpha_{22} = 2\times10^{-10}, \quad \alpha_{12} = \alpha_{21} = 10^{-10} \tag{68}$$

$$\text{neutral coupling } (C=1): \quad \alpha_{ij} = 10^{-10} \tag{69}$$

$$\text{strong coupling } (C>1): \quad \alpha_{11} = \alpha_{22} = 10^{-10}, \quad \alpha_{12} = \alpha_{21} = 2\times10^{-10} \tag{70}$$

In selecting appropriate pump parameters g_{ij}, five different pump levels were defined:

well above threshold:	$g_{21} > 2h_1$	$g_{22} > 2h_2$
slightly above threshold:	$h_1 < g_{21} < 1.1h_1$	$h_2 < g_{22} < 1.1h_2$
threshold:	$g_{21} = h_1$	$g_{22} = h_2$
slightly below threshold:	$0.9h_1 < g_{21} < h_1$	$0.9h_2 < g_{22} < h_2$
well below threshold:	$g_{21} < 0.5h_1$	$g_{22} < 0.5h_2$

For each pump level, both $g_{21} = g_{22}$ and $g_{21} > g_{22}$ were considered. For the case of $g_{21} > g_{22}$, the values were chosen so that mode 2 was

totally inhibited by mode 1. This corresponds to n_2 being negative at the equilibrium defined by (48). The values chosen for the pump parameters are found in Table I, as well as the other laser parameter values previously mentioned.

The only other variable in the laser rate equations which must be specified is the size of the system, Ω. The only restriction on Ω is that it be some finite, positive value. Therefore, for convenience, a size of $\Omega = 1$ was chosen.

Selection of Initial Conditions

For each set of laser parameters the final step before running the program and plotting the results was to determine a series of initial value points in (n_1, n_2) and their associated variances. The general goal was to select between 20 and 25 starting points per set of parameters spread around the n_1 vs. n_2 plot area. To do this required the determination of a maximum photon number NMAX which then became the dimension (in (n_1, n_2) space) for the square plotting area. For cases with pump levels above threshold, NMAX was taken to be the maximum intercept value of l_1 and l_2 as defined by (45) and (46). For threshold and below threshold cases, NMAX was determined by identifying the stable equilibrium for the particular case and multiplying the larger n- coordinate by an arbitrary factor between approximately three and ten. This ensured that the stable equilibrium was within the plotting area, but was not obscured by the axes. The values chosen for NMAX, as shown in Table I, were constant for each pump level, regardless of the degree of coupling. Initial points were then selected evenly around the edge of the plotting area in addition to several points around the origin and points close to any pre-determined unstable equilibria.

Table I. Laser Parameter Values

Pump Level	Weak Coupling		Strong Coupling		Neutral Coupling
	matched	unmatched	matched	unmatched	unmatched
well above NMAX = 4×10^{10}	A11 $g_{ij} = 5.0\times10^{8}$	A12 $g_{21} = 5.0\times10^{8}$ $g_{22} = 2.5\times10^{8}$	A13 $g_{ij} = 5.0\times10^{8}$	A14 $g_{21} = 5.0\times10^{8}$ $g_{22} = 2.5\times10^{8}$	A15 $g_{21} = 5.0\times10^{8}$ $g_{22} = 2.5\times10^{8}$
slightly above NMAX = 8×10^{8}	A21 $g_{ij} = 1.08\times10^{8}$	A22 $g_{21} = 1.08\times10^{8}$ $g_{22} = 1.02\times10^{8}$	A23 $g_{ij} = 1.08\times10^{8}$	A24 $g_{21} = 1.08\times10^{8}$ $g_{22} = 1.02\times10^{8}$	A25 $g_{21} = 1.08\times10^{8}$ $g_{21} = 1.02\times10^{8}$
threshold NMAX = 1.8×10^{5}	A31 $g_{ij} = 10^{8}$		A33 $g_{ij} = 10^{8}$		A35 ** $g_{ij} = 10^{8}$
slightly below NMAX = 250	A41 $g_{ij} = 0.98\times10^{8}$	A42 $g_{21} = 0.98\times10^{8}$ $g_{22} = 0.92\times10^{8}$	A43 $g_{ij} = 0.98\times10^{8}$	A44 $g_{21} = 0.98\times10^{8}$ $g_{22} = 0.92\times10^{8}$	A45 $g_{21} = 0.98\times10^{8}$ $g_{22} = 0.92\times10^{8}$
well below NMAX = 16	A51 $g_{ij} = 0.5\times10^{8}$	A52 $g_{21} = 0.6\times10^{8}$ $g_{22} = 0.1\times10^{8}$	A53 $g_{ij} = 0.5\times10^{8}$	A54 $g_{21} = 0.6\times10^{8}$ $g_{22} = 0.1\times10^{8}$	A55 $g_{21} = 0.6\times10^{8}$ $g_{22} = 0.1\times10^{8}$
	$\alpha_{11} = \alpha_{22} = 2.0\times10^{-10}$ $\alpha_{12} = \alpha_{21} = 1.0\times10^{-10}$ $h_1 = h_2 = 10^{8}$		$\alpha_{11} = \alpha_{22} = 1.0\times10^{-10}$ $\alpha_{11} = \alpha_{22} = 2.0\times10^{-10}$ $h_1 = h_2 = 10^{8}$		$\alpha_{11} = \alpha_{22} = \alpha_{12} = \alpha_{21} = 10^{-10}$ $h_1 = h_2 = 10^{8}$

** matched modes
A__ identification by which each set of conditions will referred in the plots

Having selected the initial (n_1, n_2), the question is how to determine, or choose, appropriate initial variances for each point. To do this, another question was asked. How would each initial point be attained physically so that the system could then make a transition to the desired stable equilibrium? One possibility is to first change some of the laser parameters such that the initial point becomes a stable equilibrium point. The system is then returned "instantaneously" to the original configuration and the behavior of the system in transition is observed. This scheme was used, varying the cavity loss terms h_1 and h_2, as in a Q-switched laser. The necessary "new" loss terms were determined by solving Eqs (36) and (37) at equilibrium for h_1 and h_2, respectively, given n_1 and n_2. Then, using these "new" values and the initial n_1 and n_2, the associated variances were obtained by solving Eqs (63), (60), and (61). In several cases (above threshold, strongly-coupled), some of the initial points could not be changed into stable equilibria by merely changing the cavity losses. In these instances, the initial values for the variances were arbitrarily set as follows:

$$\sigma_{11} = n_1^2 \tag{71a}$$

$$\sigma_{22} = n_2^2 \tag{71b}$$

$$\sigma_{12} = -n_1 n_2 \tag{71c}$$

In running the computer program to determine the behavior of the laser system, it was decided that the standard deviations s_1 and s_2 and the correlation coefficient defined by

$$s_1 = \sqrt{\sigma_{11}} \quad , \qquad s_2 = \sqrt{\sigma_{22}} \tag{72}$$

and

$$\rho_{12} = \frac{\sigma_{12}}{\sqrt{\sigma_{11}\,\sigma_{22}}} \tag{73}$$

would be of more interest than the actual variances. Therefore, these values were calculated and printed out along with the photon densities, the variances, and XOUT each time the program cycled through the BLCKDQ loop. In addition, besides the n_1 vs. n_2 plots similar to Lamb's results, three-dimensional plots involving s_1, s_2, and ρ_{12} were produced.

IV Results and Discussion

Equilibrium Analysis

Photon Densities. The photon density equilibrium points for each combination of laser parameter values (as defined in Table I) are listed in Table II. Included is the classification of each point. As expected, there are generally four such points for each set. The only exception is when the modes are neutrally coupled (i.e., when the cross-coupling terms equal the self-saturation terms). In this case, there are either two or three singular points, depending on whether the pump parameters are equal or unequal, respectively. For all but the threshold cases, these points are very close to the equilibria of the noiseless approximation (as defined by Eqs (41) and (42)). The difference, though small, is important because it indicates that a photon vacuum is never an equilibrium, stable or unstable, for either mode. Therefore, even when there is no net gain for the system, there is some positive average-photon-density to which the system will relax.

For each set of parameters, there is at least one stable and one unstable node. The type of the other singularities depends on both the degree of coupling and the level of pump. For all weak and neutral coupled cases, these other equilibria are all saddle points, each of which has one negative coordinate thus ensuring that the system can move toward stability from any physically realizeable point. When the laser modes are strongly coupled, the type of these other singularities is determined by the level of pumping. At threshold, these two equilibria are both complex-valued. Below threshold, both singularities are unstable, one being a saddle point and the other an unstable node

Table II. Classification of Photon Density Singular Points

Data Set ID	n_1	n_2	Type
A11	1.333×10^{10}	1.333×10^{10}	stable node
	2.000×10^{10}	-2.500	saddle
	-2.500	2.000×10^{10}	saddle
	-1.250	-1.250	unstable node
A12	2.000×10^{10}	5.000	stable node
	-1.538	7.500×10^{9}	saddle
	2.167×10^{10}	-3.333×10^{9}	saddle
	-1.250	-1.667	unstable node
A13	4.000×10^{10}	1.250	stable node
	1.333×10^{10}	1.333×10^{10}	saddle
	1.250	4.000×10^{10}	stable node
	-1.250	-1.250	unstable node
A14	4.000×10^{10}	0.3846	stable node
	-5.000	1.500×10^{10}	saddle
	-3.333×10^{9}	2.167×10^{10}	stable spiral
	-1.250	-1.667	unstable node
A15	4.000×10^{10}	1.000	stable node
	-2.003	1.500×10^{10}	saddle
	-1.250	-1.667	unstable node
A21	4.000×10^{8}	-27.000	saddle
	-27.000	4.000×10^{8}	saddle
	2.667×10^{8}	2.667×10^{8}	stable node
	-13.500	-13.500	unstable node
A22	4.000×10^{8}	51.000	stable node
	-15.429	1.000×10^{8}	saddle
	4.667×10^{8}	-1.333×10^{8}	saddle
	-13.500	-51.000	unstable node

Table II. Classification of Photon Density Singular Points (cont)

Data Set ID	n_1	n_2	Type
A23	8.000×10^8	13.500	stable node
	13.500	8.000×10^8	stable node
	2.667×10^8	2.667×10^8	saddle
	-13.500	-13.500	unstable node
A24	8.000×10^8	7.286	stable node
	-27.000	2.000×10^8	saddle
	-1.333×10^8	4.667×10^8	stable spiral
	-13.500	-51.000	unstable node
A25	8.000×10^8	17.000	stable node
	-18.000	2.000×10^8	saddle
	-13.5000	-51.000	unstable node
A31	1.000×10^5	-1.000×10^5	saddle
	-1.000×10^5	1.000×10^5	saddle
	5.7735×10^4	5.7735×10^4	stable node
	-5.7735×10^4	5.7735×10^4	unstable node
A33	5.7735×10^4	5.7735×10^4	stable node
	-5.7735×10^4	-5.7735×10^4	unstable node
	$1.000 \times 10^5 i$	$-1.000 \times 10^5 i$	complex
	$-1.000 \times 10^5 i$	$1.000 \times 10^5 i$	complex
A35	7.0711×10^4	7.0711×10^4	stable node
	-7.0711×10^4	7.0711×10^4	unstable node
A41	49.000	49.000	stable node
	-6.667×10^7	-6.667×10^7	unstable node
	-1.000×10^8	98.000	saddle
	98.000	-1.000×10^8	saddle
A42	49.000	11.500	stable node
	-49.000	-4.000×10^8	unstable node
	-1.000×10^8	13.143	saddle
	1.333×10^8	-4.667×10^8	saddle

Table II. Classification of Photon Density Singular Points (cont)

Data Set ID	n_1	n_2	Type
A43	49.000	49.000	stable node
	-6.667×10^{7}	-6.667×10^{7}	saddle
	-2.000×10^{8}	-49.000	unstable node
	-49.000	-2.000×10^{8}	unstable node
A44	49.000	11.500	stable node
	-2.000×10^{8}	23.000	saddle
	-7.000	-8.000×10^{8}	unstable node
	-4.667×10^{8}	1.333×10^{8}	unstable spiral
A45	49.000	11.5000	stable node
	-2.000×10^{8}	15.333	saddle
	-16.333	-8.000×10^{8}	unstable node
A51	1.000	1.000	stable node
	-1.667×10^{9}	-1.667×10^{9}	unstable node
	-2.500×10^{9}	2.000	saddle
	2.000	-2.500×10^{9}	saddle
A52	1.500	0.1111	stable node
	-11.994	-4.500×10^{9}	unstable node
	-2.000×10^{9}	0.1429	saddle
	3.333×10^{8}	-4.667×10^{9}	saddle
A53	1.000	1.000	stable node
	-1.667×10^{9}	-1.667×10^{9}	saddle
	-5.000×10^{9}	-1.000	unstable node
	-1.000×10^{9}	-5.000×10^{9}	unstable node
A54	1.500	0.1111	stable node
	-4.000×10^{9}	1.000	saddle
	-4.667×10^{9}	3.333×10^{8}	unstable spiral
	-0.4286	-9.000×10^{9}	unstable node
A55	1.500	0.1111	stable node
	-4.000×10^{9}	0.2000	saddle
	-1.200	-9.000x109	unstable node

or an unstable spiral. Above threshold, when the two modes are pumped equally, there is a second stable node which is physically realizeable. The fourth singularity is a saddle point lying essentially at the intersection of lines l_1 and l_2 (Eqs (43) and (44)). Given the initial conditions, it determines to which stable node the system will relax. When only one mode is inhibited, the second stable equilibrium point moves to a non-physical point and becomes a stable spiral. The saddle moves to a point just outside the physical region and maintains its relative position between the two stable points to prevent physical points from relaxing towards the non-physical stable point.

Second Moments. For each photon density singularity, there is one set of equilibrium values for the second moments (as determined by Eqs (60), (61), and (63)). For the unstable photon-density-equilibria, the associated second-moment equilibria are non-physical; at least one of the variances, ρ_{11} or ρ_{22}, is negative. However, since the points are unstable in the photon densities, the uncertainties and thus the second moments will grow or diverge in time, and the system will move away from instead of towards these non-physical variances.

For the stable photon singularities, the associated second-moment equilibria are real, physically meaningful points. As such, they are listed in Table III along with the associated relative standard deviations and correlation coefficients. At and below threshold the system experiences large uncertainties as the standard deviations are of the same order as the photon number densities. These large uncertainties are also experienced by modes above threshold which are inhibited by the other mode from lasing. Once a mode begins lasing, the relative standard deviation at equilibrium drops sharply, decreasing as the

Table III. Stable Equilibrium Values for the First and Second Moments of the Photon Density Distribution

Data Set ID	n_1	n_2	σ_{11}	σ_{22}	σ_{12}	Relative s_1	Relative s_2	ρ_{12}
A11	1.33×10^{10}	1.33×10^{10}	3.33×10^{10}	3.33×10^{10}	-1.67×10^{10}	1.37×10^{-5}	1.37×10^{-5}	-.5000
A12	2.00×10^{10}	5.000	2.50×10^{10}	30.00	-16.72	7.91×10^{-6}	1.095	-1.931×10^{-5}
A13	4.00×10^{10}	1.250	5.00×10^{10}	2.813	-4.732	5.59×10^{-6}	1.342	-1.26×10^{-5}
A14	4.00×10^{10}	0.3846	5.00×10^{10}	0.5325	-0.8405	5.59×10^{-6}	1.892	-5.15×10^{-6}
A15	4.00×10^{10}	1.000	5.00×10^{10}	2.000	-2.000	5.59×10^{-6}	1.414	-6.325×10^{-6}
A21	2.67×10^{8}	2.67×10^{8}	7.20×10^{9}	7.20×10^{9}	-3.60×10^{9}	3.18×10^{-4}	3.18×10^{-4}	-.5000
A22	4.00×10^{8}	51.00	5.40×10^{9}	2.65×10^{3}	-1.33×10^{3}	1.84×10^{-4}	1.010	-3.53×10^{-4}
A23	8.00×10^{8}	13.50	1.08×10^{10}	195.8	-378.5	1.30×10^{-4}	1.037	-2.60×10^{-4}
A24	8.00×10^{8}	7.286	1.08×10^{10}	60.37	-115.6	1.30×10^{-4}	1.066	-1.43×10^{-4}
A25	8.00×10^{8}	17.00	1.08×10^{10}	306.0	-306.0	1.30×10^{-4}	1.029	-1.68×10^{-4}
A31	5.77×10^{4}	5.77×10^{4}	2.08×10^{9}	2.08×10^{9}	-4.17×10^{8}	.7905	.7905	-.2000
A33	5.77×10^{4}	5.77×10^{4}	3.33×10^{9}	3.33×10^{9}	-1.67×10^{9}	1.000	1.000	-.5000
A35	7.07×10^{4}	7.07×10^{4}	3.75×10^{9}	3.75×10^{9}	-1.25×10^{9}	.8660	.8660	-.3333

Table III. Stable Equilibrium Values for the First and Second Moments of the Photon Density Distribution (cont.)

Data Set ID	n_1	n_2	σ_{11}	σ_{22}	σ_{12}	Relative s_1	Relative s_2	ρ_{12}
A41	49.00	49.00	2450	2450	-6.00×10^{-4}	1.010	1.010	-2.45×10^{-7}
A42	49.00	11.50	2450	143.7	-3.52×10^{-5}	1.010	1.042	-5.935×10^{-8}
A43	49.00	49.00	2450	2450	-1.20×10^{-3}	1.010	1.010	-4.900×10^{-7}
A44	49.00	11.50	2450	143.7	-7.04×10^{-5}	1.010	1.042	-1.19×10^{-7}
A45	49.00	11,50	2450	143.7	-3.52×10^{-5}	1.010	1.042	-5.935×10^{-8}
A51	1.000	1.000	2.000	2.000	-4.00×10^{-10}	1.414	1.414	-2.00×10^{-10}
A52	1.500	0.1111	3.750	0.1235	-4.63×10^{-11}	1.291	3.163	-6.80×10^{-11}
A53	1.000	1.000	2.000	2.000	-8.00×10^{-10}	1.414	1.414	-4.00×10^{-10}
A54	1.500	0.1111	3.750	0.1235	-9.26×10^{-11}	1.291	3.163	-1.36×10^{-10}
A55	1.500	0.1111	3.750	0.1235	-4.63×10^{-11}	1.291	3.163	-6.80×10^{-11}

photon number density increases. It is interesting to note that for a weakly-coupled system above threshold, matched-mode oscillation ($n_1 = n_2$) shows for each of the modes a greater variance than for the single mode that oscillates and inhibits the other. This is even though, for the same pump level, the photon density is greater for the single mode than for either of the matched modes. However, this general phenomenon should be expected because of the relative influences of the second mode; in one case, it oscillates at equal intensity while in the other instance it exists barely above photon vacuum.

The correlation coefficient ρ_{12} indicates a significant linear relationship between the photon densities of the two modes only at threshold and above thresold with both modes lasing. In these cases a change in the photon density of one mode will have definite impact on the density of the other. At threshold, even though the standard deviations are still on the order of the mean densities, this indicates the onset of order within the system. Below threshold, and above threshold with only one mode oscillating, ρ_{12} is very small and the two modes are very nearly uncorrelated. Below threshold, both modes are dominated by spontaneous emission. Therefore, neglecting the small amount of stimulated emission that may occur, the photons in one mode will have no effect on the photon number in the other mode. Likewise, above threshold with one inhibiting the other, the inhibited mode is inhabited almost entirely by spontaneous photons and can do very little to affect the number density of the lasing mode.

Dynamic Analysis

General. Representative plots showing the evolution of the mean photon number densities and of the standard deviations and correlation

coefficient are shown in Figs. 6-13. Each figure comprises four plots: n_1 vs. n_2; n_1 vs. n_2 vs. s_1; n_1 vs. n_2 vs. s_2; and n_1 vs. n_2 vs. ρ_{12}. There were no significant differences in the behavior of the system between the two levels of above threshold pump considered in this study. Therefore, only one of these pump levels is considered in this section. The same was true for the two levels of pump below threshold. In addition, the degree of coupling had no real noticeable effect below threshold on the evolution of the variables and caused only minor differences at threshold. Therefore, only one threshold case and two below threshold cases (corresponding to matched and unmatched pumping) are considered. The remainder of the plots are included in Appendix C.

Below Threshold. Figs. 6 and 7 illustrate the evolution of the first and second moments for the two below threshold cases A41 and A42, respectively. As predicted, the mean photon densities follow deterministic paths. In both cases the modes are dominated by spontaneous emission. Therefore, they exhibit characteristics of white (incoherent) light. The standard deviations s_1 and s_2 are on the order of the mean densities throughout the transitions and, therefore, experience the same general behavior as the mean photon densities. Also, the correlation coefficient is very near zero throughout the regions of interest indicating that the modes have little on each other.

At Threshold. At threshold, only the weakly-coupled case A31 has real-valued saddle points. The strongly-coupled system A33 has two complex-valued singularities, while the neutrally-coupled system A35 has only two nodes, one stable and one unstable. Comparing these three cases, it is seen that there is little impact caused by the presence (or absence) of saddle points.

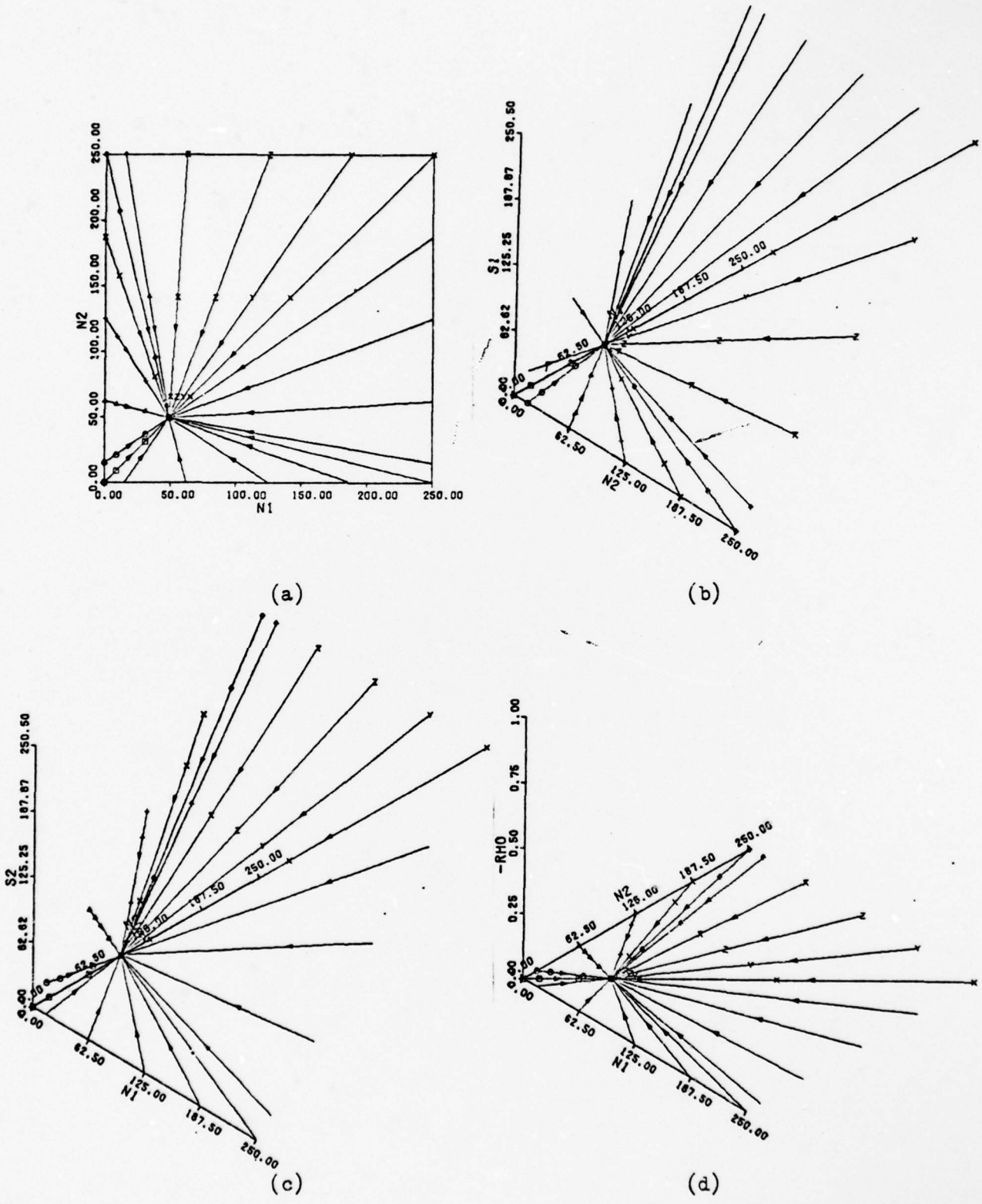

Figure 6. Evolution Curves for Case A41

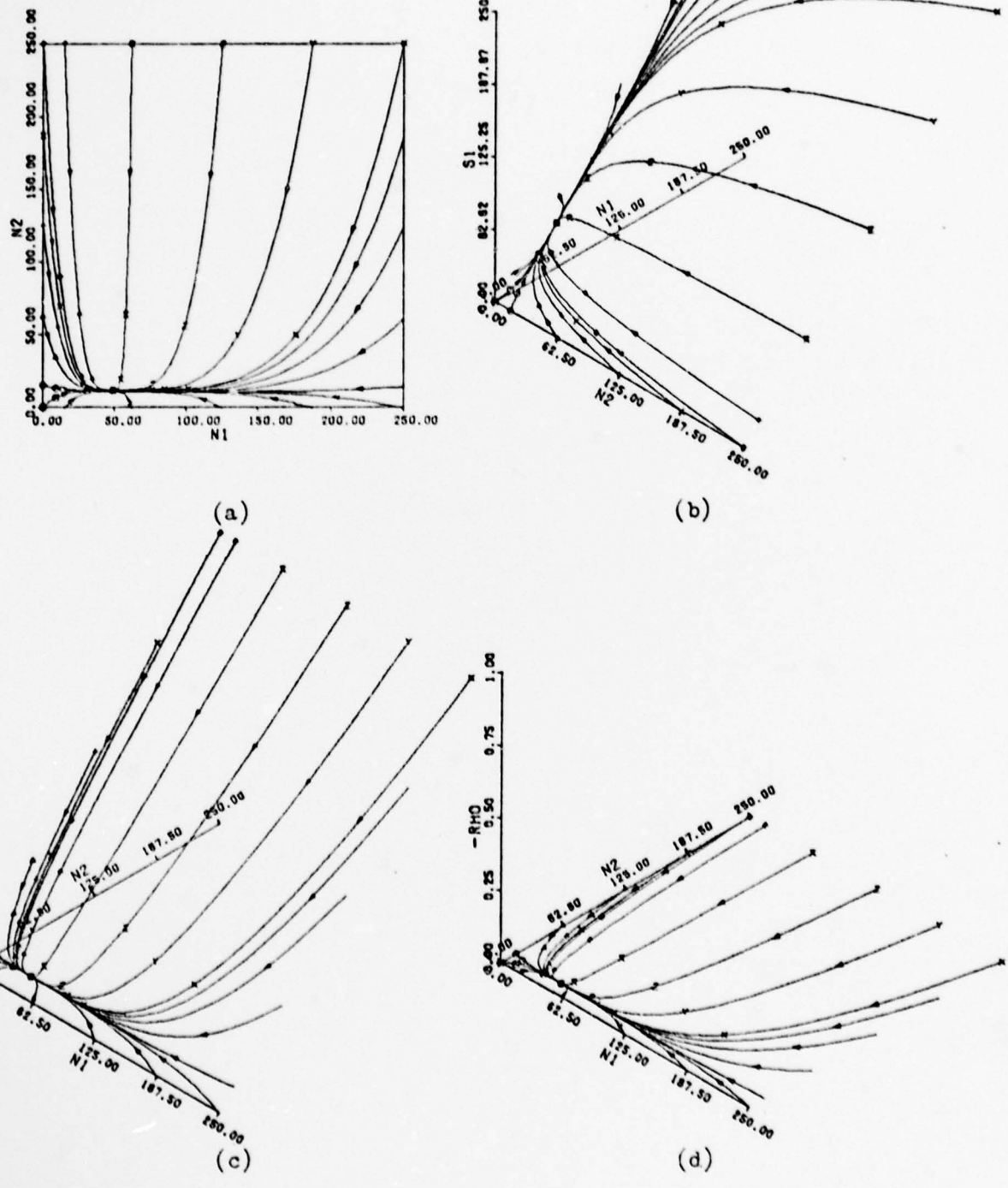

Figure 7. Evolution Curves for Case A42

Considering the case A35 (Fig. 8), the same general relationships exist between the mean photon densities and the standard deviations as exist below threshold. The modes are still dominated primarily by spontaneous emission and, therefore, s_1 and s_2 remain on the order of n_1 and n_2. However, the correlation coefficient no longer is negligible. When either mode is operating well below equilibrium the correlation between modes is very small. As the mode(s) grow(s), the effects of saturation and coupling cause the modes to affct each other and thus they become correlated. Because of the simulated Q-switch used to determine the initial variances and covariances, the curves associated with large initial photon densities in both modes start out indicating significant correlation between modes which then decrease or increase monotonically towards the equilibrium value.

Above Threshold. Above threshold, the behavior of the system is strongly affected by the singular points (Table II). Consider first the weakly-coupled case A21 as shown in Fig. 9. Comparing Fig. 9a, the plot of n_1 vs. n_2, to Fig 1, its equivalent plot resulting from Lamb's semiclassical treatment, favorable agreement is noted with an important addition. Fig. 9a includes phase curves from points with one or both modes in a photon vacuum. The curves between the saddle points at approximately $(0,4\text{x}10^8)$ and $(4\text{x}10^8,0)$ and the stable equilibrium act as "limit lines" of the system to which other phase curves are pulled by the saddle points. This is especially evident for those lines beginning with one of the modes in a photon vacuum (such as those with initial points identified on the n_2 axis by several different characters). These curves move quickly towards the closest saddle point before the non-lasing mode can build significantly, as there are not enough excited

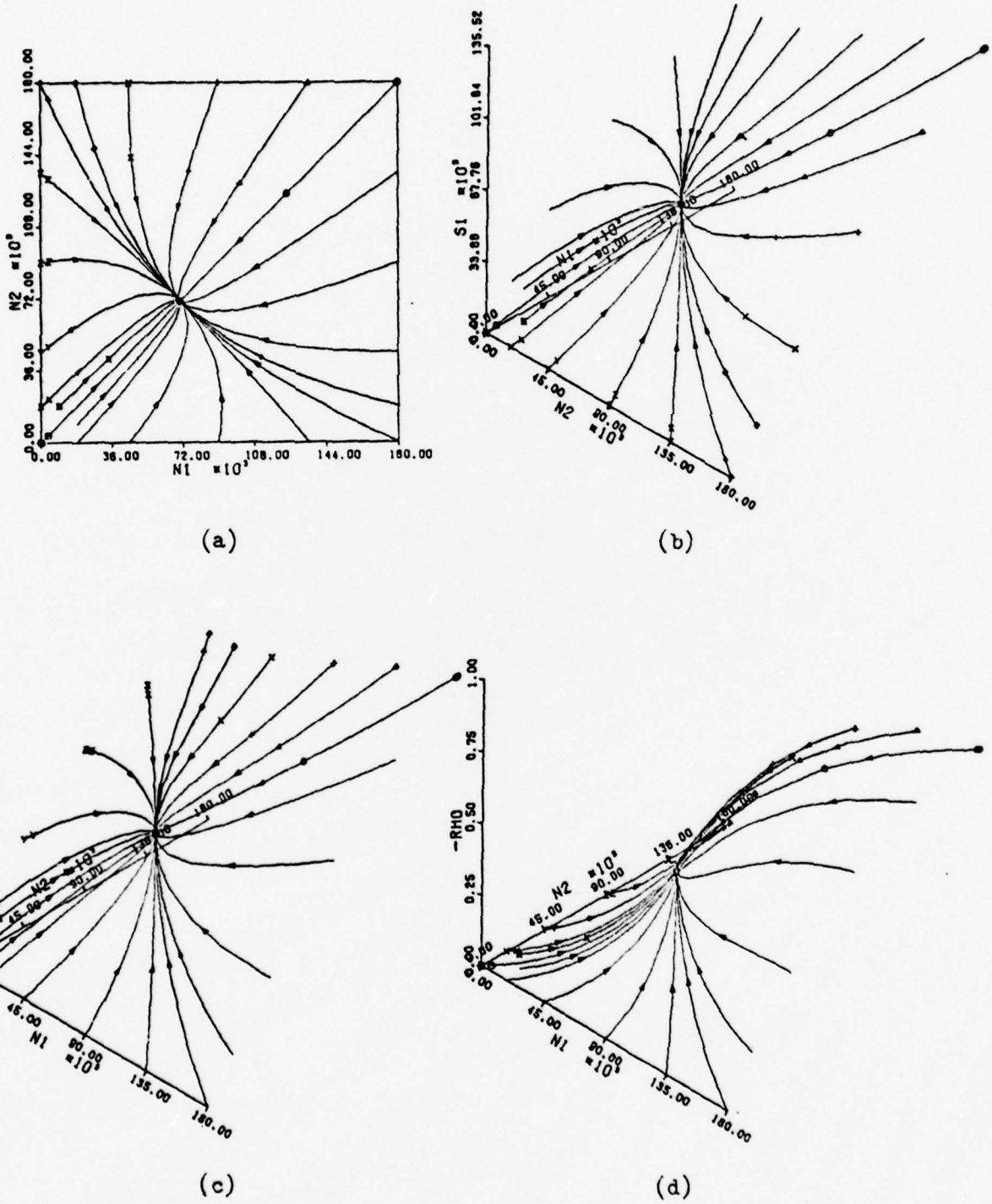

Figure 8. Evolution Curves for Case A35

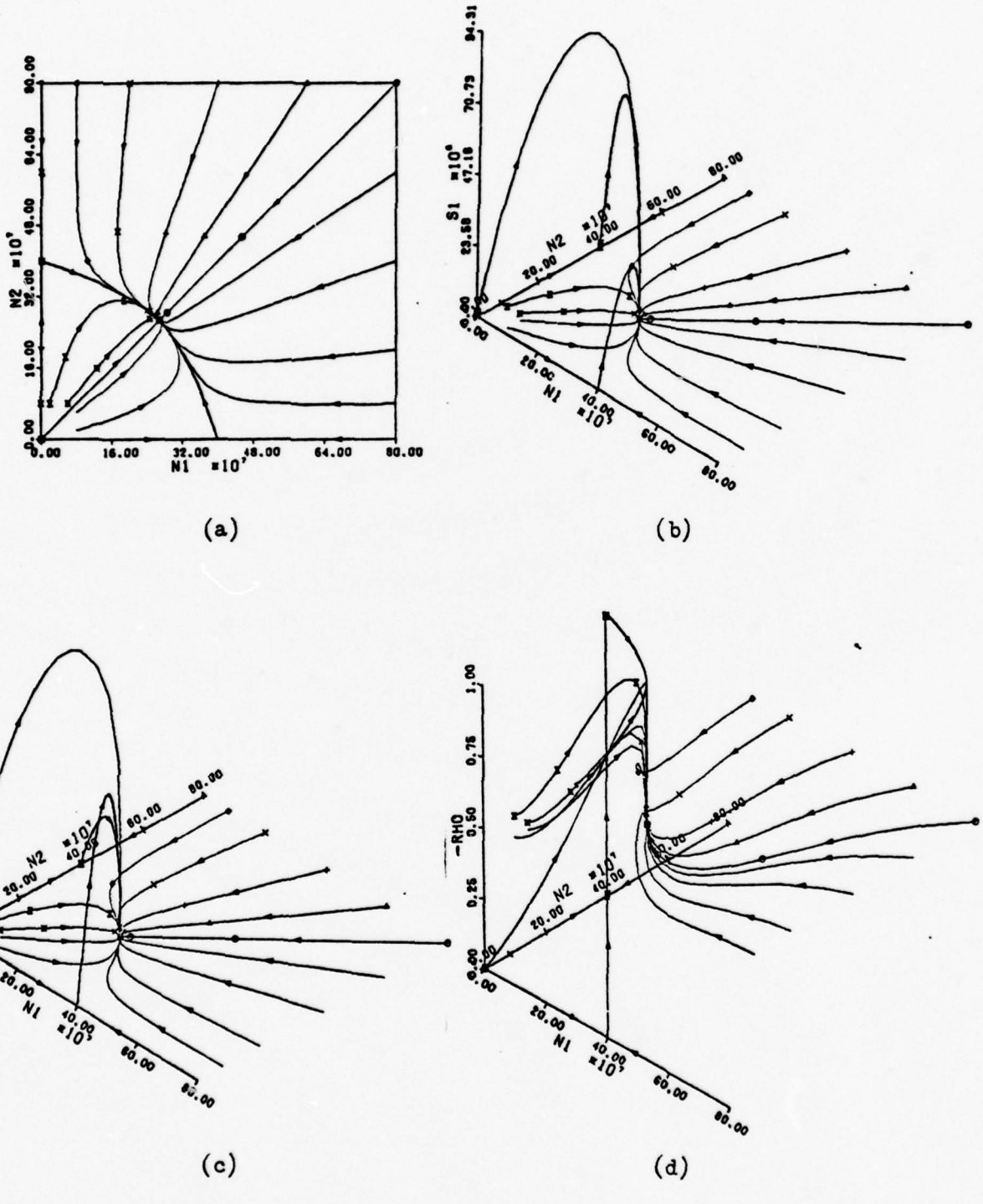

Figure 9. Evolution Curves for Case A21

atoms to maintain the system at its current level. They then follow very closely the "limit line" in the transition to stable equilibrium. Figs. 9b and 9c indicate that the occurence of anomalous fluctuations is associated with buildup in one or both modes from a photon vacuum, and that the maximum fluctuation occurs approximately half-way along the curve between the stable and unstable equilibria. In buildup from $(n_1, n_2) = (0, 0)$ both modes experience the same degree of fluctuation as both modes are expected to grow at the same rate. When only one mode is building from zero both modes again experience the anomalously large fluctuations, even though the other mode is already oscillating. However, the growing mode experiences a larger fluctuation. Comparing the curves for s_1 and s_2 to their associated curves for ρ_{12} in Fig. 9d, it is seen that movement along the "limit line" is associated with a high correlation between modes ($\rho_{12} \approx -1.0$). Also, the phase curve associated with buildup from a photon vacuum in both modes moves towards $\rho_{12} = -1.0$ before relaxing to the equilibrium value of -0.5.

Case A22, representing weakly-coupled modes with mode 2 inhibited at equilibrium, is shown in Fig. 10. As with case A21, a comparison of Fig. 10a with its equivalent from Lamb's theory (Fig. 2) indicates favorable agreement in n_1 and n_2. There is now only one saddle point, at $(n_1, n_2) \approx (0, 10^8)$, which affects the system and all phase curves move toward the one equilibrium where only mode 1 lases. The anomalously large fluctuations are again associated with buildup from a photon vacuum. The single-to-dual-mode transition of Fig. 9 is replaced by transition from unstable to stable mode oscillation, and again both modes experience the anomalous fluctuations, as seen in Figs. 10b and 10c. However, only mode 1 experiences anomalous fluctuations in build-

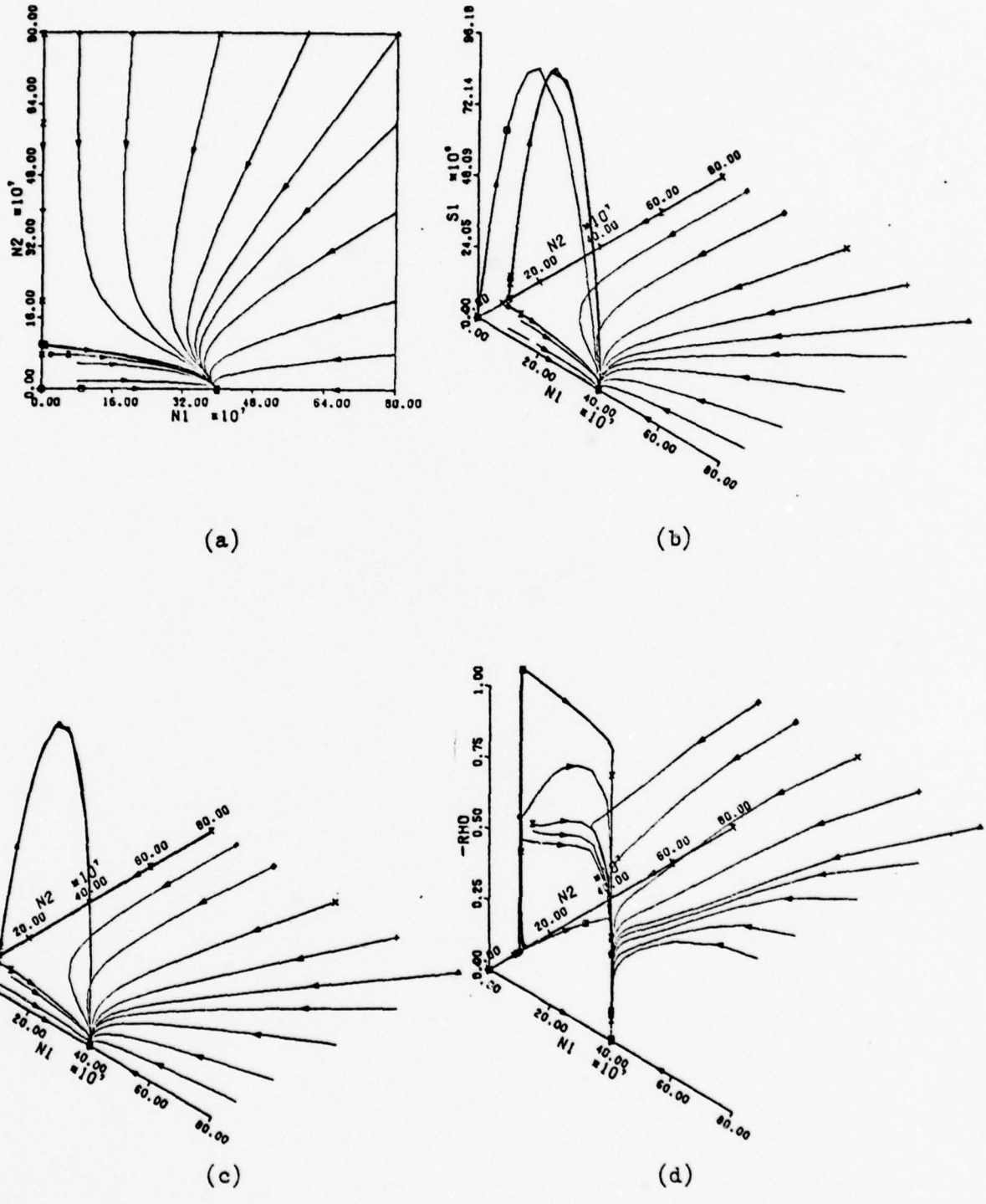

Figure 10. Evolution Curves for Case A22

up from (0,0) since it is the only mode which oscillates at equilibrium. Also, movement along or close to the "limit line" is again associated with strong correlation between the modes, as illustrated in Fig. 10d.

The case of strongly-coupled modes pumped equally, as shown in Fig. 11, is unique from the other cases studied because it has two different equilibria which are stable nodes and to which the system can relax. It also has an unstable equilibrium lying in the physical region of the (n_1,n_2) plane. This internal saddle point determines the stable point to which the system will move. As before, the evolution of the mean photon densities, Fig. 11a, compares favorably with Lamb's results as plotted in Fig. 3. Since both modes can be stable, depending on one's current position, the system does not have an unstable mode from which to transition, as in case A22. Similarly, it cannot move to two-mode oscillation. Therefore, one might expect that for this case the only anomalous fluctuations are associated with buildup in one of the modes from a photon vacuum while the other mode remains essentially empty. However, while photon buildup transitions do experience the anomalous fluctuations, the strongest influence is the internal saddle point. As is evident in Figs. 11b and 11c, the phase curves experiencing the largest fluctuations are those passing closest to this saddle point. Again, it is interesting to note that the maximum fluctuations occur not nearest the unstable equilibrium, but approximately half-way between the unstable point and the stable point. As in all the above-threshold cases studied, movement along the "limit lines" extending between the stable and unstable equilibria was associated with high correlation between the modes, or $\rho_{12} = -1.0$. However, for strongly-coupled modes, due to the stronger mode interaction, this same correlation exists

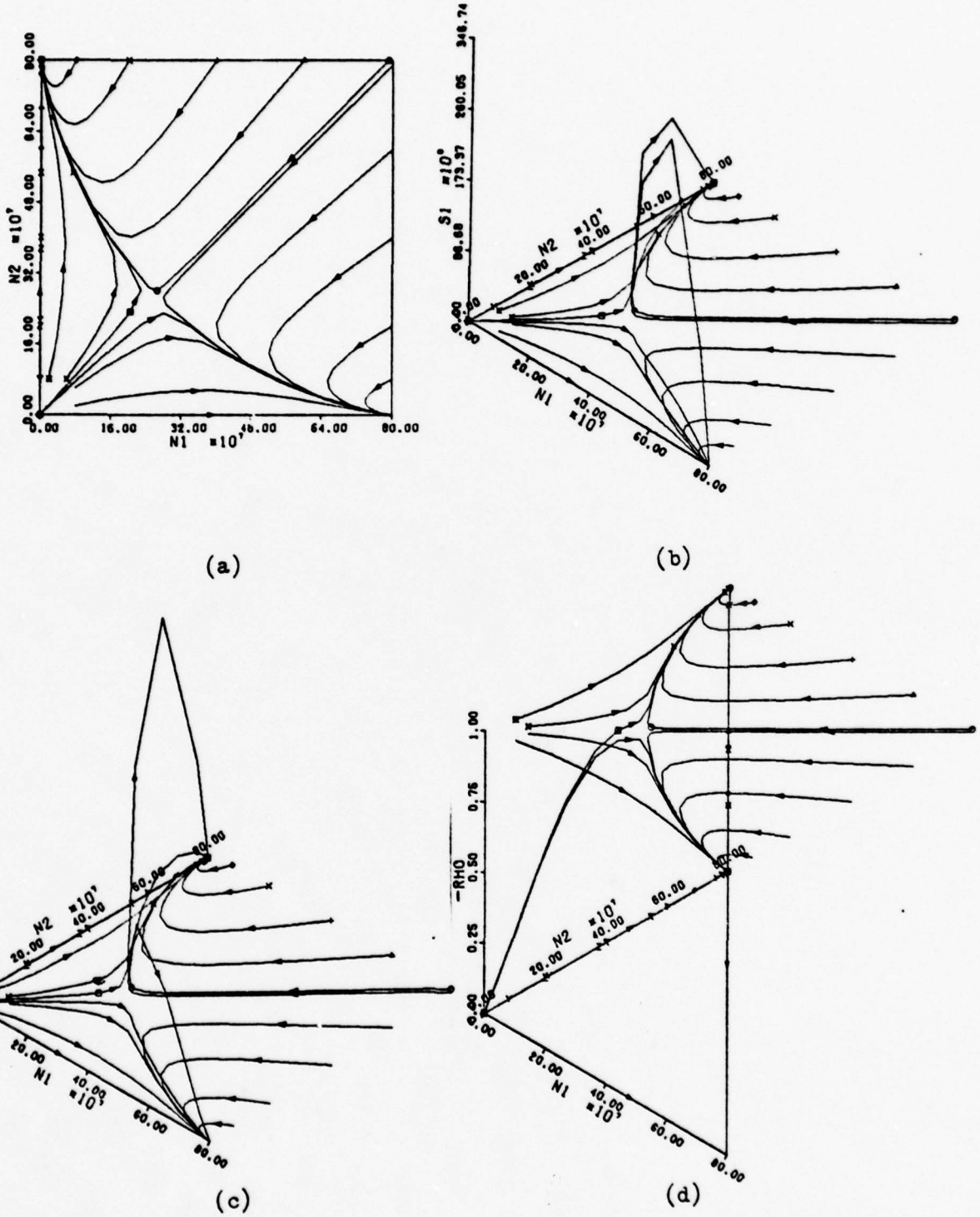

Figure 11. Evolution Curves for Case A23

whenever both modes are oscillating, as seen in Fig. 11d.

When the strongly-coupled modes are unequally pumped such that only one mode is inhibited, as in case A24, the evolution of the moments is as shown in Fig. 12. There is again only one stable point to which the system can relax and there is only one saddle point affecting the system. As in case A22, anomalous fluctuations occur during both transition from unstable to stable mode oscillation and buildup of mode 1 from a photon vacuum (0,0). However, the largest fluctuations are associated with phase curves which begin with both modes oscillating and then pass near the saddle point. Both modes oscillating under strong coupling is a highly unstable configuration and, therefore, the curves associated with these points begin with large uncertainties on the order of the mean photon densities. As the system evolves toward the stable equilibrium, s_2 maintains the same relative value throughout the transition (Fig. 12c). Likewise, for those curves which approach the "limit line" before the half-way point where the maximum fluctuations are expected to occur, s_1 stays on the order of n_1 and as n_1 grows, so does s_1 (Fig. 12b). Once the maximum point is reached, s_1 decreases rapidly and approaches its relative low value characteristic of stable lasing modes.

Looking at Fig. 13, there are only minor differences between the evolution curves for neutrally-coupled modes and those for strongly-coupled modes under unequal pumping. For the neutrally-coupled modes (case A25) the effect of the saddle point is not as pronounced. The phase curves do not approach as close to the saddle point and, excepting those which begin on the n_2 axis, do not approach the "limit line" as quickly. Therefore, even though the two-mode-oscillation initial points have associated uncertainties on the order of the photon densities,

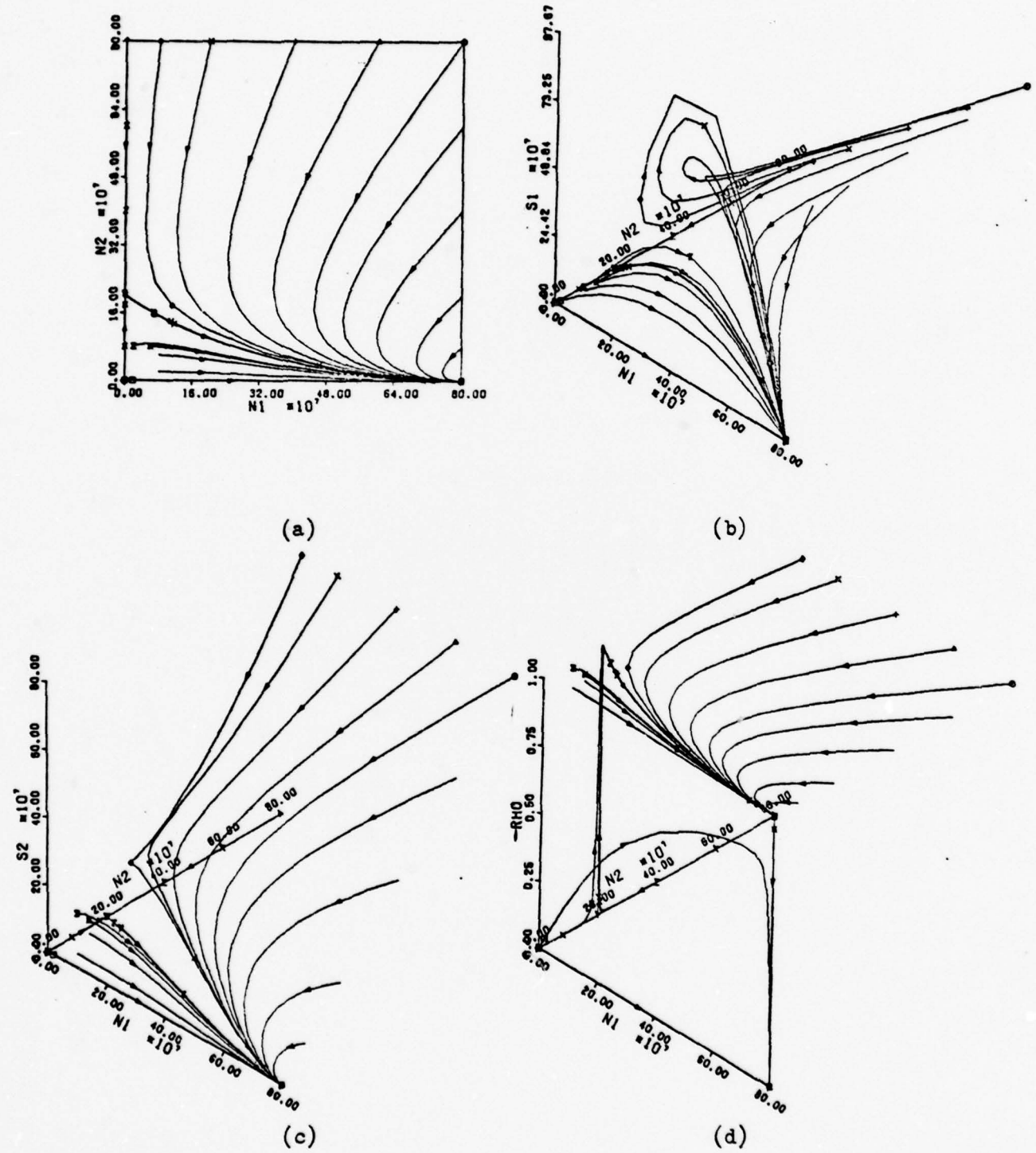

Figure 12. Evolution Curves for Case A24

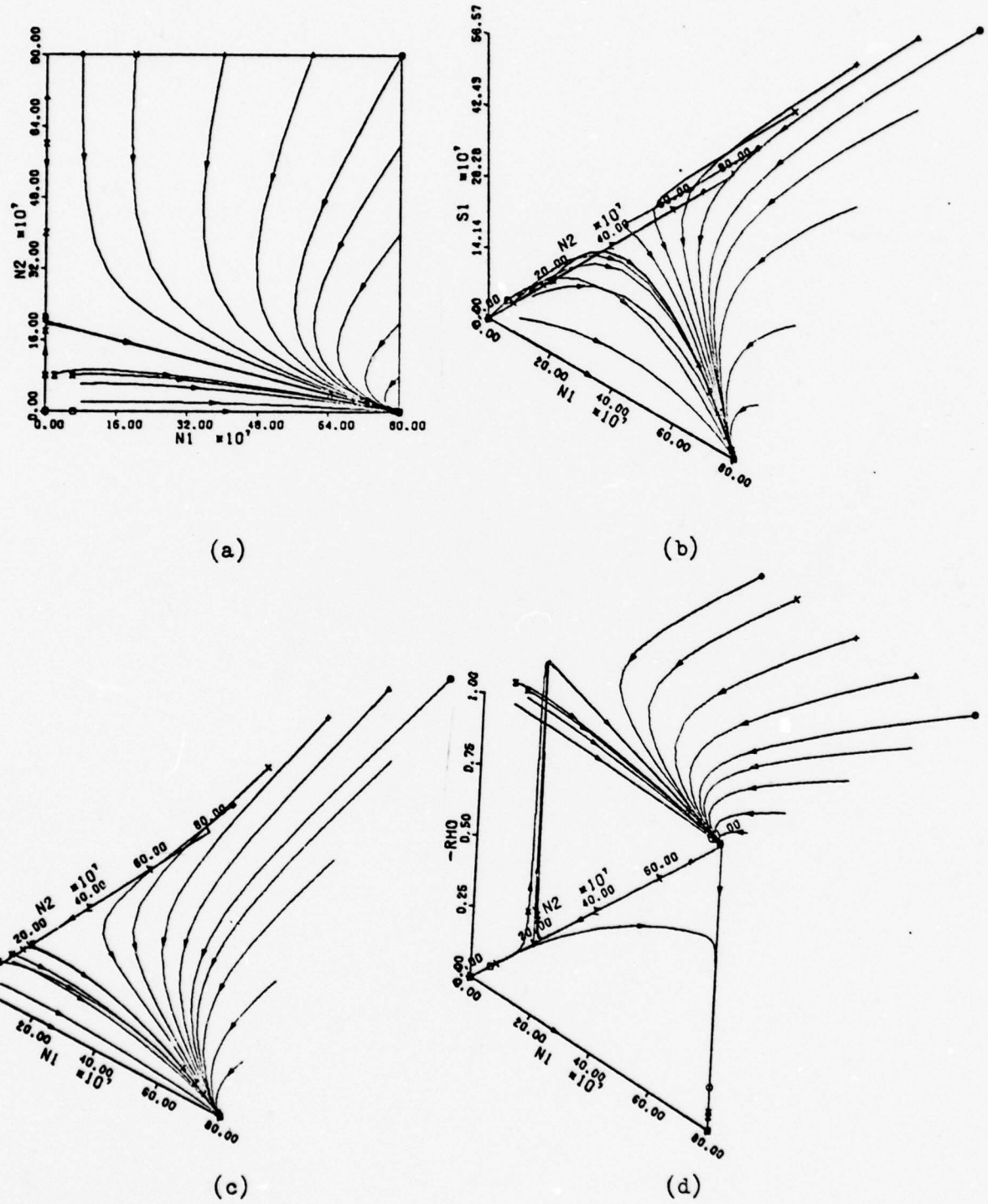

Figure 13. Evolution Curves for Case A25

the loops in the s_1 curves of Fig. 12b do not occur in the s_1 curves of Fig. 13b.

It is interesting to look at the general shape of the "limit lines" relative to the mode coupling. When the modes are weakly coupled and and the system is in the vicinity of a saddle point, one of the mode densities will be near zero. As this mode grows, the other mode density will decrease as both modes pull towards their own respective equilibria. However, the decrease required will be less than the growth of the first mode. Therefore, the "limit lines" are concave downward or towards the origin. On the other hand, the "limit lines" are concave upward for strongly-coupled modes as the opposite relative responses between modes are encountered. When the system is neutrally-coupled, the "limit line" becomes a straight line showing no preferred concavity, just as the system shows no preferred method of saturation.

In comparing Figs. 9a, 10a, and 11a to the results of Lamb's theory (Figs. 1, 2, and 3) the one important difference noted was the inclusion of phase curves originating from a photon vacuum. There is one other significant difference between these two models. Lamb's model predicted that any point along lines l_1 and l_2 (Eqs (43) and (44)) would be stable with deviations away from either line decaying back towards that line. However, when the spontaneous emission is included, this stability is destroyed and, as seen in Fig. 13, the system moves to equilibrium at a single point.

Mode Buildup from Vacuum. Of particular interest is the buildup of the mode densities from a photon vacuum. Figs. 14a, 14b, and 14c illustrate this buildup in time for several levels of pump and degrees of coupling. Fig. 14c shows the buildup in both modes from a photon

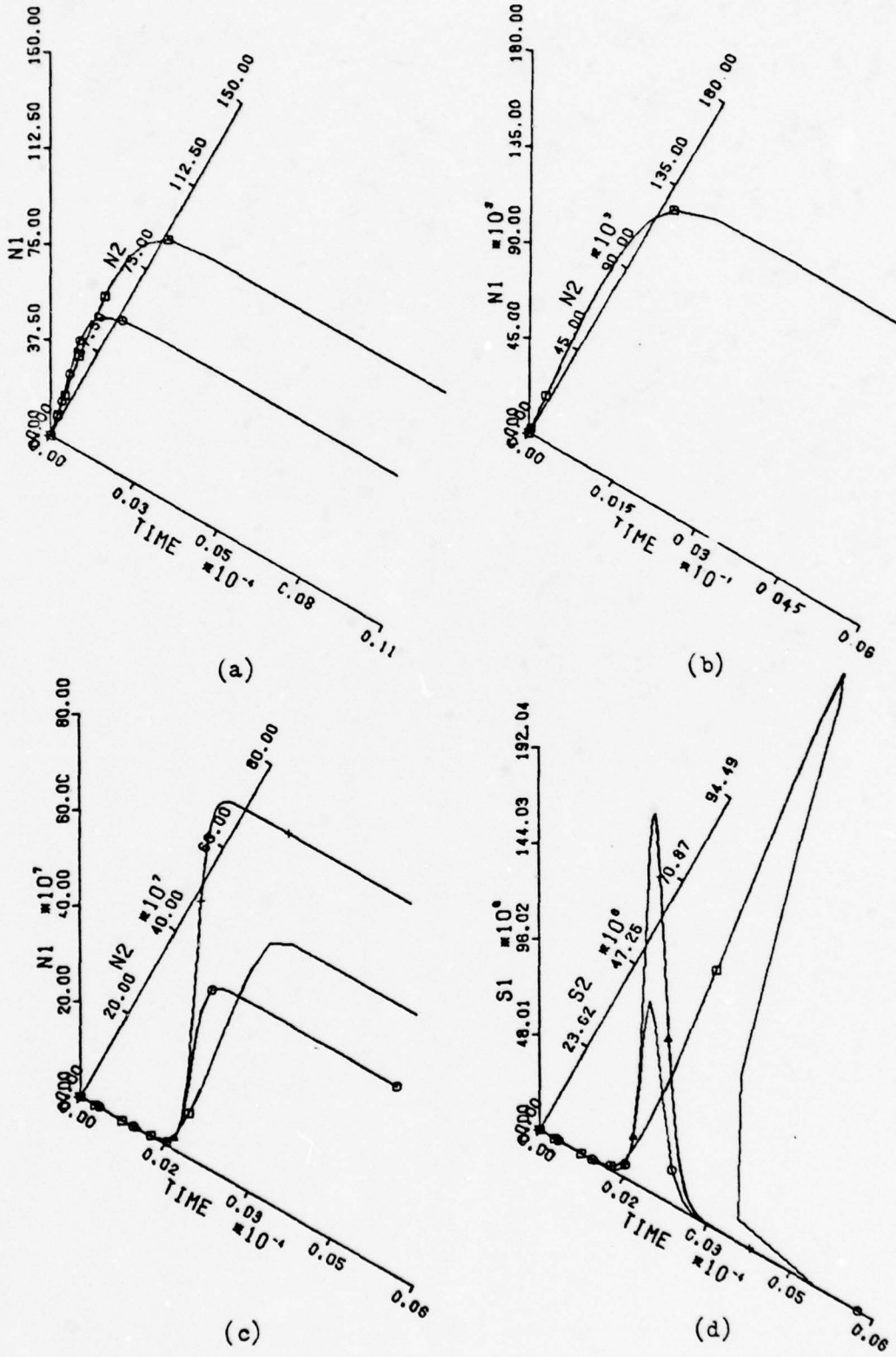

Figure 14. Time Evolution of Moments During Buildup of Photon Densities

vacuum for the five different above threshold cases shown in Figs. 9-13. Fig. 14b corresponds to Fig 8, and Fig. 14a does the same for the cases of Figs. 6 and 7. Below threshold, the modes grow independently with the time relationship

$$n_i = n_{i_{eq}}\left(1 - e^{-at}\right) \tag{74}$$

where $n_{i_{eq}}$ is the equilibrium density for that mode and a_i is a decay constant. This decay constant is equal to the net losses of the mode, or the difference between the loss parameter h_i and the stimulated gain parameter g_{2i}. Coupling and saturation have negligible effects. At threshold, according to Eq (74) both modes should increase linearly with no damping or aplification effects, since the stimulated gains equal the losses. This does occur initially. However, as the mode densities continue to increase, saturation sets in and the rate of buildup declines as equilibrium is reached. Above threshold, both modes experience initial exponential rises with growth constants equal to the net gain of the system. As they approach and pass the threshold equilibria, saturation and coupling begin to modify this rise, gradually slowing the rate of increase and even causing a decrease for the mode which is inhibited from lasing at equilibrium.

The time to equilibrium is primarily determined by the size of the net gain or loss of the system. The closer the system is to threshold operation, the longer it will take for the system to buildup to equilibrium. Below threshold, the net loss (or the decay constant) is the only determining factor, whereas above threshold, and even at threshold, the effects of coupling and inhibition speed up or slow down the process.

For example, consider the times to equilibria as shown in Figs. 14a-14c. At threshold (Fig. 14b), this time was on the order of 1 msec. Below threshold (Fig 14a), it took about 5μsec for the system to reach an equilibrium. In Fig. 14c the times to equilibrium were in the range of 5-10μsec.

As with the photon densities, the buildup of the mode densities is used to illustrate the evolution of the standard deviations in time. See Fig. 14d. Since the standard deviations for systems at and below threshold are very close to the mean photon densities, only the above threshold cases represented in Fig 14c are considered. Also, the strongly-coupl. equally-pumped system experienced fluctuations two orders of magnitude greater than the fluctuations for the other four cases involved. Therefore, the time behavior of its standard deviations is not included in Fig. 14d. Comparing the curves of Fig. 14d to Fig 14c, it is seen that the fluctuations do peak approximately half-way to equilibrium, as predicted and seen before, with the case of two-mode oscillation peaking farther towards the equilibrium than the cases of single-mode oscillation. The height of the peak is dependent primarily on the pumping, as different pump parameters produce different photon densities. There is also a dependence on the mode coupling for the same pump level. For each of the curves in Fig 14d, the peak represents approximately the same relative standard deviation ($s_i \approx n_i$). Therefore, since the peak occurs when the photon density is about half that of the equilibrium value, the heights of the peaks will have the same relative values as do the equilibrium photon densities.

V Conclusions and Recommendations

Conclusions

Based on the results of this study, several conclusions can be drawn. The most important of these, without which the rest would be meaningless, is that the method used in this study of photon statistics is valid. The lasing process can be described adequately by the Chapman-Kolmogorov master equation and the proposed transition rates used in solving the master equation are appropriate. Accepting this, the other conclusions are;

1). Any two-mode laser system has at most two stable equilibria, with all but some strongly-coupled systems having only one. This includes systems with neutrally-coupled modes, contrary to the predictions of the Lamb model.

2). The laser system experiences large, anomalous fluctuations in one or both modes in three specific types of transition. First, whenever the system builds up from a near photon vacuum such as at initial startup, the mode or modes which will be oscillating at equilibrium will experience the anomalous fluctuations. Second, whenever only one mode is oscillating and both modes oscillate at equilibrium, both modes will experience the anomalous fluctuations during the transition to equilibrium. Third, whenever an unstable mode is oscillating alone both modes will have anomalous fluctuations in the transition from the unstable to the stable mode.

3). Strongly-coupled laser systems operating with two modes oscillating experience large fluctuations, especially when there are two possible stable points to which the laser system can transition.

4). A mode experiences normal fluctuations when the system is below threshold, when the mode both begins and ends the transition below threshold, and when one mode ceases lasing while the other mode continues to lase (excepting the case where two physical stable points exist).

5). Inhibited modes above threshold experience the same type of fluctuation as if they were below threshold.

6). The anomalous fluctuations are accompanied by a strong linear relationship between the mode densities ($\rho_{12} \approx -1$).

7). There is significant correlation at equilibrium between the modes only at threshold and above threshold with both modes oscillating.

Recommendations for Further Study

1). A better qualitative understanding of the effect of coupling could be gained by solving several different cases for various values of the coupling parameters.

2). Operation very close to threshold should be given a closer look, possibly resulting in a better definition of "near threshold".

3). This study was limited to constant pump parameters which turned on or changed instantaneously. Therefore, a similar analysis could be done allowing the pump parameters to be functions of time. This could then allow for analysis of pulsed operation as well as continuous wave.

4). This analysis could be repeated for other proposed expressions for the transition rates.

5). The equation development used in this study should be expanded to include multimode laser operation and the general results for two-mode operation extended as appropriate.

Bibliography

1. Arecchi, F. T. and A. M. Ricca. "Statistical Properties of a Many-Mode Laser," Physical Review A, 15: 308-318 (January 1977).

2. Arecchi, F. T. et al. "Time-Dependent Statistical Properties of the Laser Radiation," Physical Review Letters, 19: 1168-1171 (13 November 1967).

3. Haken, H. "Cooperative Phenomena in Systems Far From Thermal Equilibrium and in Nonphysical Systems," Reviews of Modern Physics, 47: 67-121 (January 1975).

4. Kubo, R. "Non-linear Relaxation," Statistical Physics--StatPhys 13, Annals of the Israel Physical Society, Vol 2, Part 1, edited by D. Cahib, et al. New York: Adam Hilger, Bristol and the Israel Physical Society in association with the American Physical Society, 1978.

5. -----. "Relaxation and Fluctuation of Macrovariables," Synergetics - Cooperative Phenomena in Multi-component Systems, edited by H. Haken. Stuttgart: Teubner, 1973.

6. Kubo, R. et al. "Fluctuation and Relaxation of Macrovariables," Journal of Statistical Physics, 9: 51-96 (September 1973).

7. Lamb, W. E., Jr. "Theory of an Optical Maser," Physical Review, 134: A1429-A1450 (15 June 1964).

8. Mandel, P. "Quantum Multi-mode Laser Theory," Physica B & C, Netherlands, 82: 353-367 (April 1976).

9. Risken, H. "Statistical Properties of Laser Light," Progress in Optics, VIII: 241-296 (1970)

10. Sargent, M. III et al. "Buildup of Laser Oscillations from Quantum Noise," Applied Optics, 9: 2423-2427 (November 1970).

11. -----. Laser Physics. Reading, Massachusetts: Addison-Wesley Publishing Co., 1974.

12. Siegman, A. E. An Introduction to Lasers and Masers. New York: McGraw-Hill Book Co., 1971.

13. Skappel, J., Boeing Aircraft. "FORTRAN IV Subroutine BLCKDQ," Coordination Sheet No. PS-769, 22 March 1968.

14. Standard Math Tables (17th Edition), edited by Samuel M. Selby. Cleveland, Ohio: The Chemical Rubber Co., 1969.

15. Stoker, J. J. Nonlinear Vibrations in Mechanical and Electrical Systems. New York: Interscience Publishers, Inc., 1950.

16. van Kampen, N. G. "A Power Series Expansion of the Master Equation," Canadian Journal of Physics, 39: 551-567 (1961).

Appendix A Derivation of the Evolution Equations

Let $\underline{X} = (X_1, X_2)$ be a vector variable representing the photon numbers of a two-mode laser system. It is assumed that $\underline{X}$ is a stochastic process as it evolves in time. Further, $\underline{X}$ is assumed to be Markovian and, therefore, can be described by the Chapman-Kolmogorov equation in the form

$$\frac{\partial}{\partial t} P(\underline{X}, t) = -\int W(\underline{X}, \underline{r}) P(\underline{X}, t) d\underline{r} + \int W(\underline{X} - \underline{r}, \underline{r}) P(\underline{X} - \underline{r}, t) d\underline{r} \quad (75)$$

where $P(\underline{X}, t)$ is the probability distribution of $\underline{X}$ at time t and $W(\underline{X}, \underline{r})$ is the transition rate for a jump from $\underline{X}$ by an amount $\underline{r}$. Since the values of $\underline{X}$ will be discrete, the integrations are understood as summations.

$\underline{X}$, as defined above, represents the extensive macrovariables of the laser system, each of which is made up of contributions from many elementary units - in this case, photons. However, it is assumed that the transition rate $W(\underline{X}, \underline{r})$ is determined by the internal state of the system, rather than by $\underline{X}$. Therefore, the transition rate takes the form

$$W(\underline{X}, \underline{r}) = \Omega \omega(\underline{x}, \underline{r}) \quad (76)$$

where Ω is the size of the system and $\underline{x}$ is the normalized intensive macrovariable vector corresponding to $\underline{X}$ and defined by

$$\underline{x} = \underline{X} / \Omega \quad (77)$$

With this assumption, the master equation (75), rewritten for $P(\underline{x},t) = \Omega P(\underline{X},t)$, becomes

$$\frac{1}{\Omega}\frac{\partial}{\partial t}P(\underline{x},t) = -\int \omega(\underline{x},\underline{r})P(\underline{x},t)d\underline{r} + \int \omega(\underline{x}-\frac{\underline{r}}{\Omega},\underline{r})P(\underline{x}-\frac{\underline{r}}{\Omega},t)d\underline{r} \quad (78)$$

By expanding the second integral on the right-hand side of Eq (78) in a power series about $\underline{x}$, Eq (78) can be written formally as

$$\frac{1}{\Omega}\frac{\partial}{\partial t}P(\underline{x},t) = -\int \left[1 - \exp\left(-\frac{\tilde{\underline{r}}}{\Omega}\cdot\underline{\nabla}\right)\right] \omega(\underline{x},\underline{r})P(\underline{x},t)d\underline{r} \quad (79)$$

or, maintaining the expanded form

$$\frac{1}{\Omega}\frac{\partial}{\partial t}P(\underline{x},t) = \sum_{n=1}^{\infty}\left(\frac{-1}{\Omega}\right)^n \frac{1}{n!}\int d\underline{r}\left(\tilde{\underline{r}}\cdot\underline{\nabla}\right)^n \omega(\underline{x},\underline{r})P(\underline{x},t) \quad (80)$$

where $\tilde{\underline{r}}$ is the transpose of $\underline{r}$.

Following the work of Kubo (Ref 5:29), a solution of Eq (80) of the form

$$P(\underline{x},t) = C\exp\left[\Omega f(\underline{x},t)\right] \quad (81)$$

is assumed. Then, the time derivative of $P(\underline{x},t)$ is

$$\frac{\partial}{\partial t}P(\underline{x},t) = \frac{\partial}{\partial t}\left[C\exp\left[\Omega f(\underline{x},t)\right]\right] = \Omega P(\underline{x},t)\frac{\partial}{\partial t}f(\underline{x},t) \quad (82)$$

and the integrand on the right-hand side of Eq (80) becomes

$$(\tilde{r}\cdot\nabla)^n \omega(\underline{x},r)P(\underline{x},t) = (\tilde{r}\cdot\nabla)^n \omega(\underline{x},r)\, C\exp\left[\Omega f(\underline{x},t)\right]$$

$$= \Omega^n \omega(\underline{x},r)P(\underline{x},t)(\tilde{r}\cdot\nabla f)^n$$

$$+ O(\Omega^{n-1}) \qquad (83)$$

Therefore, to order Ω^0 , Eq (80) becomes

$$\frac{\partial}{\partial t} f(\underline{x},t) = \sum_{n=1}^{\infty} (-1)^n \frac{1}{n!} \int dr\, \omega(\underline{x},r)(\tilde{r}\cdot\nabla f)^n \qquad (84)$$

and (79) becomes

$$\frac{\partial}{\partial t} f(x,t) = -\int dr\, \omega(\underline{x},r)\left[1 - \exp(-\tilde{r}\cdot\nabla f(\underline{x},t))\right] \qquad (85)$$

To solve this equation, a solution of the form

$$f(\underline{x},t) = g(\underline{z},t) \quad , \quad \underline{x} = \underline{y}(t) + \underline{z} \qquad (86)$$

is assumed, where $\underline{y}(t)$ is the expected value of $\underline{x}$ and $\underline{z}$ is the deviation of $\underline{x}$ away from $\underline{y}$. This, then, transforms (85) into

$$\frac{\partial}{\partial t} g(\underline{z},t) - \dot{\tilde{y}}(t)\cdot\nabla_z g(\underline{z},t) = -\int dr\, \omega(\underline{y}+\underline{z},r)\left[1 - \exp(-\tilde{r}\cdot\nabla g)\right] \qquad (87)$$

Assuming $|\underline{z}| << |\underline{y}(t)|$, the transition rate $w(\underline{y}+\underline{z},\underline{r})$ can be written as

$$\omega(\underline{y}+\underline{z},r) = \omega(\underline{y},r) + \tilde{z}\cdot\nabla_y \omega(\underline{y},r) + \ldots \qquad (88)$$

which then transforms (87) into

$$\frac{\partial}{\partial t} g(\underline{z},t) - \dot{\underline{\tilde{y}}} \cdot \nabla_{\underline{z}} g(\underline{z},t) = -\int d\underline{r}\, p\, \omega(\underline{y},\underline{r}) \left[1 - \exp\left(-\underline{\tilde{r}} \cdot \nabla_{\underline{y}}\right)\right] g$$

$$- \int d\underline{r}\, p\, \underline{\tilde{\underline{z}}} \cdot \nabla_{\underline{y}} \omega(\underline{y},\underline{r}) \left[1 - \exp\left(-\underline{\tilde{r}} \cdot \nabla_{\underline{y}}\right)\right] g \qquad (89)$$

Expanding the exponential terms, Eq (89) becomes

$$\frac{\partial}{\partial t} g(\underline{z},t) - \dot{\underline{\tilde{y}}} \cdot \nabla_{\underline{z}} g(\underline{z},t) = \sum_{n=1}^{\infty} \frac{(-1)^n}{n!} \int d\underline{r}\, p\, \omega(\underline{y},\underline{r}) \left(\underline{\tilde{r}} \cdot \nabla_{\underline{y}}\right)^n g$$

$$+ \underline{\tilde{z}} \cdot \nabla_{\underline{y}} \sum_{n=1}^{\infty} \frac{(-1)^n}{n!} \int d\underline{r}\, p\, \omega(\underline{y},\underline{r}) \left(\underline{\tilde{r}} \cdot \nabla_{\underline{z}}\right)^n g \qquad (90)$$

Noting that the first moment of the transition, $\int d\underline{r}\, \omega(\underline{y},\underline{r})\, \underline{r}$, is just the average velocity of $\underline{y}$ when the system is in the state $\underline{y}$, and that $\underline{y}(t)$ is already an average or expected value, it is easily seen that $\underline{y}(t)$ satisfies the condition

$$\dot{\underline{y}}(t) = \int d\underline{r}\, p\, \omega(\underline{y},\underline{r})\, \underline{r} \qquad (91)$$

Therefore, the terms in Eq (90) linear in $\nabla_{\underline{z}} g(\underline{z},t)$ vanish and the resultant equation is

$$\frac{\partial}{\partial t} g(\underline{z},t) = \sum_{n=2}^{\infty} \frac{(-1)^n}{n!} \int d\underline{r}\, p\, \omega(\underline{y},\underline{r}) \left(\underline{\tilde{r}} \cdot \nabla_{\underline{z}}\right)^n g$$

$$+ \underline{\tilde{z}} \cdot \nabla_{\underline{y}} \sum_{n=1}^{\infty} \frac{(-1)^n}{n!} \int d\underline{r}\, p\, \omega(\underline{y},\underline{r}) \left(\underline{\tilde{r}} \cdot \nabla_{\underline{z}}\right)^n g \qquad (92)$$

Assuming an approximate gaussian solution of

$$g(\underline{z},t) = -\frac{1}{2}\,\tilde{\underline{z}}\cdot\underline{\underline{\Lambda}}(t)\cdot\underline{z} + O(|\underline{z}|^3) \tag{93}$$

where $\underline{\underline{\Lambda}}$ is the inverse of the covariance tensor, then

$$\begin{aligned}\tilde{\underline{r}}\cdot\nabla_z g(\underline{z},t) &= -\frac{1}{2}\,\tilde{\underline{r}}\cdot\nabla_z\left(\tilde{\underline{z}}\cdot\underline{\underline{\Lambda}}(t)\cdot\underline{z}\right) + O(|\underline{z}|^3)\\ &= -\frac{1}{2}\,r_\alpha\frac{\partial}{\partial z_\alpha}\left(z_\beta\Lambda_{\beta\gamma}z_\gamma\right) + O(|\underline{z}|^3)\\ &= -\frac{1}{2}\,r_\alpha\Lambda_{\alpha\gamma}z_\gamma - \frac{1}{2}\,r_\alpha z_\beta\Lambda_{\beta\alpha} + O(|\underline{z}|^3)\end{aligned} \tag{94}$$

However

$$\Lambda_{\alpha\beta} = \Lambda_{\beta\alpha} \tag{95}$$

and, therefore

$$\begin{aligned}\tilde{\underline{r}}\cdot\nabla_z g(\underline{z},t) &= -r_\alpha\Lambda_{\alpha\beta}z_\beta + O(|\underline{z}|^3)\\ &= -\tilde{\underline{r}}\cdot\underline{\underline{\Lambda}}\cdot\underline{z} + O(|\underline{z}|^3)\end{aligned} \tag{96}$$

Inserting (93) and (96) into Eq (92) and taking the leading terms to order $|\underline{z}|^2$, Eq (92) becomes

$$\begin{aligned}-\frac{1}{2}\,\tilde{\underline{z}}\cdot\dot{\underline{\underline{\Lambda}}}\cdot\underline{z} &= \frac{1}{2}\,\tilde{\underline{z}}\cdot\underline{\underline{\Lambda}}\cdot\int d\underline{r}\;\omega(\underline{y},\underline{r})\,\underline{r}\tilde{\underline{r}}\cdot\underline{\underline{\Lambda}}\cdot\underline{z}\\ &\quad+\tilde{\underline{z}}\cdot\nabla_y\int d\underline{r}\;\omega(\underline{y},\underline{r})\,\tilde{\underline{r}}\cdot\underline{\underline{\Lambda}}\cdot\underline{z}\end{aligned} \tag{97}$$

This leads directly to

$$\dot{\underline{\underline{\Lambda}}}(t) = -\underline{\underline{\Lambda}} \cdot \int d\underline{r}\, \omega(\underline{y},\underline{r})\, \underline{r}\underline{\tilde{r}} \cdot \underline{\underline{\Lambda}} - 2\nabla_y \int d\underline{r}\, \omega(\underline{y},\underline{r})\, \underline{\tilde{r}} \cdot \underline{\underline{\Lambda}} \quad (98)$$

which can then be made symmetric (recovering the symmetry lost by using (95) to combine the terms of Eq (94) by noting again the equivalence of Eq (95). Therefore

$$\nabla_y \int d\underline{r}\, \omega(\underline{y},\underline{r})\, \underline{\tilde{r}} \cdot \underline{\underline{\Lambda}} = \underline{\underline{\Lambda}} \cdot \overbrace{\left(\nabla_y \int d\underline{r}\, \omega(\underline{y},\underline{r})\, \underline{\tilde{r}}\right)} \quad (99)$$

and Eq (98) becomes

$$\dot{\underline{\underline{\Lambda}}}(t) = -\underline{\underline{\Lambda}} \cdot \int d\underline{r}\, \omega(\underline{y},\underline{r})\, \underline{r}\underline{\tilde{r}} \cdot \underline{\underline{\Lambda}} - \nabla_y \int d\underline{r}\, \omega(\underline{y},\underline{r})\, \underline{\tilde{r}} \cdot \underline{\underline{\Lambda}} - \underline{\underline{\Lambda}} \cdot \overbrace{\left(\nabla_y \int d\underline{r}\, \omega(\underline{y},\underline{r})\, \underline{\tilde{r}}\right)} \quad (100)$$

An equivalent expression for the covariance tensor $\underline{\underline{B}}(t)$ is obtained by first noting several tensor identities. By definition

$$\underline{\underline{B}} = \underline{\underline{\Lambda}}^{-1} \quad (101)$$

and, therefore

$$\underline{\underline{B}}\,\underline{\underline{\Lambda}} = \underline{\underline{E}} \quad (102)$$

where $\underline{\underline{E}}$ is the identity tensor. Taking the time derivative of Eq (102)

$$\dot{\left(\underline{\underline{B}}\,\underline{\underline{\Lambda}}\right)} = \underline{\underline{\Lambda}}\,\dot{\underline{\underline{B}}} + \underline{\underline{B}}\,\dot{\underline{\underline{\Lambda}}} = 0 \quad (103)$$

which leads to

$$\dot{\underline{\underline{B}}} = -\underline{\underline{B}} \wedge \underline{\underline{B}} \tag{104}$$

Defining $\underline{c}_1(\underline{y})$ and $\underline{\underline{c}}_2(\underline{y})$ as the first and second moments of the transition rate $w(\underline{y},\underline{r})$

$$\tilde{\underline{c}}_1(\underline{y}) = \int d\underline{r}\, w(\underline{y},\underline{r})\,\tilde{\underline{r}} \tag{105}$$

$$\underline{\underline{c}}_2(\underline{y}) = \int d\underline{r}\, w(\underline{y},\underline{r})\,\underline{r}\tilde{\underline{r}} \tag{106}$$

and inserting (100) into Eq (104), the equation for the covariance tensor is

$$\dot{\underline{\underline{B}}}(t) = \underline{\underline{c}}_2(\underline{y}) + \underline{\underline{B}}\,\nabla_y \tilde{\underline{c}}_1(\underline{y}) + \widetilde{\left(\nabla_y \tilde{\underline{c}}_1(\underline{y})\right)}\,\underline{\underline{B}} \tag{107}$$

or

$$\dot{B}_{\alpha\beta}(t) = c_{2\alpha\beta}(\underline{y}) + B_{\alpha\gamma}\frac{\partial}{\partial y^\gamma} c_{1\beta}(\underline{y}) + \frac{\partial}{\partial y^\gamma} c_{1\alpha}(\underline{y})\, B_{\gamma\beta} \tag{108}$$

To obtain the covariance tensor for $\underline{x}$, (107) must be divided by . This is seen by first inserting (93) into (87) to get (keeping only the leading term in $|\underline{z}|^2$)

$$P(\underline{x},t) = C \exp\left[-\tfrac{1}{2}\,\Omega\,\tilde{\underline{z}}\cdot\underline{\underline{\Delta}}\cdot\underline{z}\right]$$

$$= C \exp\left[-\tfrac{1}{2}\,\tilde{\underline{z}}\cdot(\Omega\underline{\underline{\Delta}})\cdot\underline{z}\right] \tag{109}$$

Letting

$$\underline{\underline{\sigma}}^{-1}(t) = \Omega \underline{\underline{\Lambda}} \tag{110}$$

be the inverse covariance tensor for $\underline{x}$, the covariance tensor becomes

$$\underline{\underline{\sigma}}(t) = \frac{1}{\Omega} \underline{\underline{B}} \tag{111}$$

Similarly

$$\underline{\underline{\lambda}}(t) = \Omega \underline{\underline{B}} \tag{112}$$

where $\underline{\underline{\lambda}}(t)$ is the covariance tensor for $\underline{X}$. Therefore, by substituting (111) back into Eq (107) the equation for the covariance tensor for $\underline{x}$ results:

$$\dot{\underline{\underline{\sigma}}}(t) = \frac{1}{\Omega} \underline{\underline{C}}_2(\underline{y}) + \underline{\underline{\sigma}}\, \nabla_y \tilde{\underline{C}}_1(\underline{y}) + \widetilde{\left(\nabla_y \tilde{\underline{C}}_1(\underline{y})\right)}\, \underline{\underline{\sigma}} \tag{113}$$

where $\underline{C}_1$ and $\underline{\underline{C}}_2$ are as defined in Eqs (105) and (106).

Thus, Eq (113) and Eq (97), which can be rewritten as

$$\dot{\underline{y}}(t) = \underline{C}_1(\underline{y}) \tag{114}$$

are the general equations governing the evolution of the first and second moments of the normalized intensive macrovariable $\underline{x}$. Equation (114) defines the most probable path $\underline{y}(t)$ which the variable $\underline{x}$ will follow, while Eq (113) determines a measure of the fluctuatims of the variable around this average path.

Appendix B Linearization of the Photon Rate Equations

To linearize the photon rate equations (36) and (37), consider a small disturbance around an equilibrium point. Let

$$n_1 = n_1^\circ + n_1' \tag{115}$$

and

$$n_2 = n_2^\circ + n_2' \tag{116}$$

where n_1° and n_2° are the equilibrium point values. Substituting these into Eq (36), the rate equation becomes

$$\dot{n}_1 = \dot{n}_1^\circ + \dot{n}_1' = \frac{g_{11} + g_{21}(n_1^\circ + n_1')}{1 + \alpha_{11}(n_1^\circ + n_1') + \alpha_{12}(n_2^\circ + n_2')} - h_1(n_1^\circ + n_1') \tag{117}$$

$$= \frac{g_{11} + g_{21}n_1^\circ + g_{21}n_1'}{1 + \alpha_{11}n_1^\circ + \alpha_{11}n_1' + \alpha_{12}n_2^\circ + \alpha_{12}n_2'} - h_1 n_1^\circ - h_1 n_1' \tag{118}$$

Now

$$\frac{1}{X + \Delta X} \approx \frac{X - \Delta X}{X^2} \tag{119}$$

Therefore, letting

$$X = 1 + \alpha_{11}n_1^\circ + \alpha_{12}n_2^\circ \tag{120}$$

and

$$\Delta X = \alpha_{11}n_1' + \alpha_{12}n_2' \tag{121}$$

Eq (118) becomes

$$\dot{n}_1' = \frac{(g_{11} + g_{21}n_1^\circ + g_{21}n_1')(1 + \alpha_{11}n_1^\circ + \alpha_{12}n_2^\circ - \alpha_{11}n_1' - \alpha_{12}n_2')}{(1 + \alpha_{11}n_1^\circ + \alpha_{12}n_2^\circ)^2} - h_1 n_1^\circ - h_1 n_1' \tag{122}$$

Separating out zero order terms

$$\dot{n}_1' = \frac{(g_{11} + g_{21} n_1^\circ)(1 + \alpha_{11} n_1^\circ + \alpha_{12} n_2^\circ - \alpha_{11} n_1' - \alpha_{12} n_2')}{(1 + \alpha_{11} n_1^\circ + \alpha_{12} n_2^\circ)^2} - h_1 n_1^\circ$$

$$+ \frac{g_{21} n_1' (1 + \alpha_{11} n_1^\circ + \alpha_{12} n_2^\circ - \alpha_{11} n_1' - \alpha_{12} n_2')}{(1 + \alpha_{11} n_1^\circ + \alpha_{12} n_2^\circ)^2} - h_1 n_1' \qquad (123)$$

$$= \left(\frac{g_{11} + g_{21} n_1^\circ}{1 + \alpha_{11} n_1^\circ + \alpha_{12} n_2^\circ} - h_1 n_1^\circ \right) \left(\frac{1 + \alpha_{11} n_1^\circ + \alpha_{12} n_2^\circ - \alpha_{11} n_1' - \alpha_{12} n_2'}{1 + \alpha_{11} n_1^\circ + \alpha_{12} n_2^\circ} \right)$$

$$+ \frac{g_{21} n_1' (1 + \alpha_{11} n_1^\circ + \alpha_{12} n_2^\circ - \alpha_{11} n_1' - \alpha_{12} n_2')}{(1 + \alpha_{11} n_1^\circ + \alpha_{12} n_2^\circ)^2} - \frac{h_1 n_1^\circ (\alpha_{11} n_1' + \alpha_{12} n_2')}{1 + \alpha_{11} n_1^\circ + \alpha_{12} n_2^\circ} - h_1 n_1' \qquad (124)$$

Now, the first bracketed factor of the first term in Eq (124) is just $\dot{n}_1^\circ$ which is equal to zero. Therefore, the entire first term vanishes and the rate equation becomes

$$\dot{n}_1' = \frac{g_{21} n_1' (1 + \alpha_{11} n_1^\circ + \alpha_{12} n_2^\circ - \alpha_{11} n_1' - \alpha_{12} n_2')}{(1 + \alpha_{11} n_1^\circ + \alpha_{12} n_2^\circ)^2} - \frac{h_1 n_1^\circ (\alpha_{11} n_1' + \alpha_{12} n_2')}{1 + \alpha_{11} n_1^\circ + \alpha_{12} n_2^\circ} - h_1 n_1' \qquad (125)$$

Since the disturbance was originally assumed to be small, only the first order terms are of significance; therefore, separating out all higher order terms, Eq (125) becomes

H.O.T. ≈ 0

$$\dot{n}_1' = \frac{g_{21} n_1' (1 + \alpha_{11} n_1^\circ + \alpha_{12} n_2^\circ)}{(1 + \alpha_{11} n_1^\circ + \alpha_{12} n_2^\circ)^2} - \frac{g_{21} n_1' (\alpha_{11} n_1' + \alpha_{12} n_2')}{(1 + \alpha_{11} n_1^\circ + \alpha_{12} n_2^\circ)^2}$$

$$- \frac{h_1 n_1^\circ (\alpha_{11} n_1' + \alpha_{12} n_2')}{1 + \alpha_{11} n_1^\circ + \alpha_{12} n_2^\circ} - h_1 n_1' \qquad (126)$$

Thus, the linearized photon rate equations are written as

$$\dot{n}_1' = \frac{g_{21} n_1' - h_1 n_1^\circ \left(\alpha_{11} n_1' + \alpha_{12} n_2'\right)}{1 + \alpha_{11} n_1^\circ + \alpha_{12} n_2^\circ} - h_1 n_1' \qquad (127)$$

and

$$\dot{n}_2' = \frac{g_{22} n_2' - h_2 n_2^\circ \left(\alpha_{22} n_2' + \alpha_{21} n_1'\right)}{1 + \alpha_{21} n_1^\circ + \alpha_{22} n_2^\circ} - h_2 n_2' \qquad (128)$$

Appendix C Additional Evolution Curves

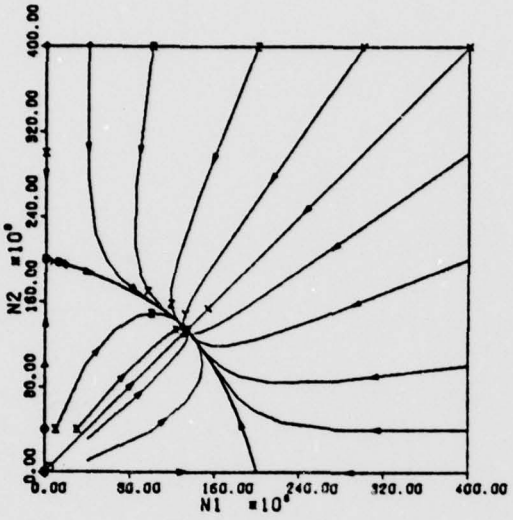

(a)

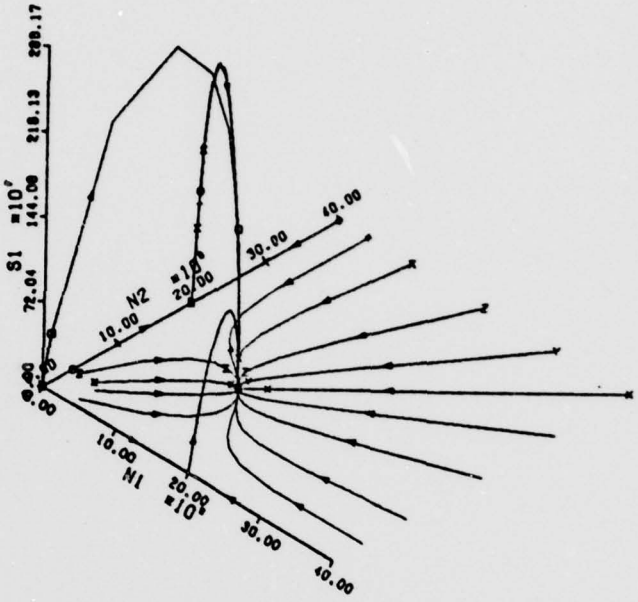

(b)

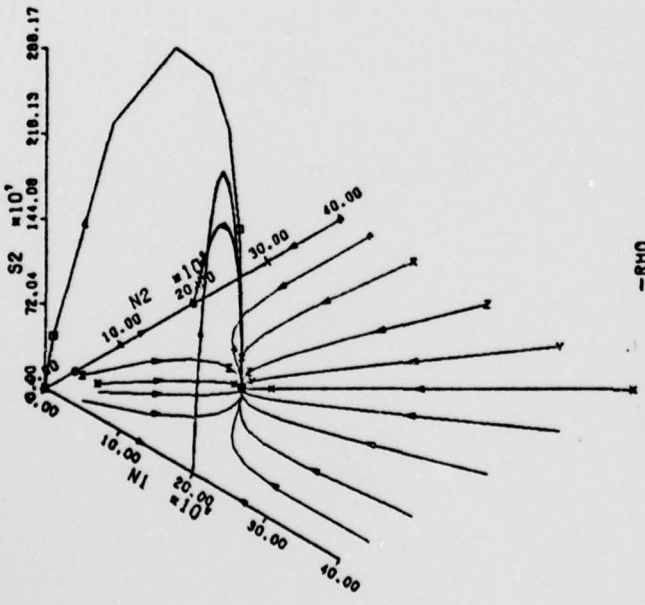

(c)

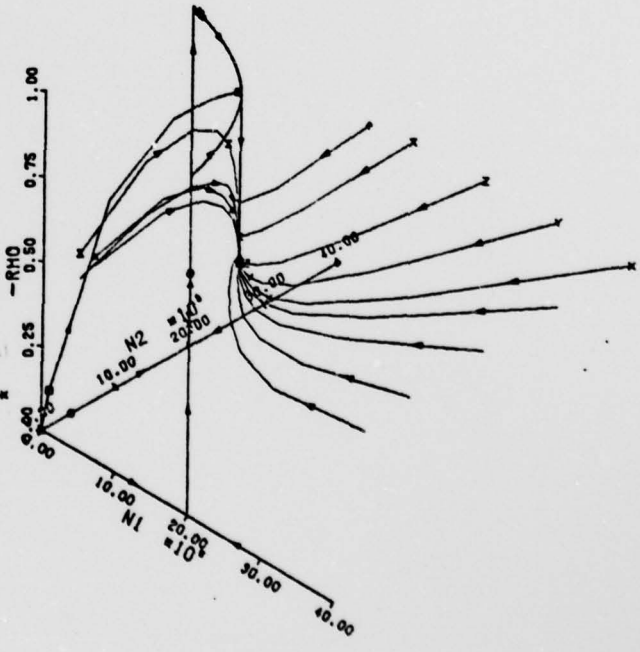

(d)

Figure 15. Evolution Curves for A11

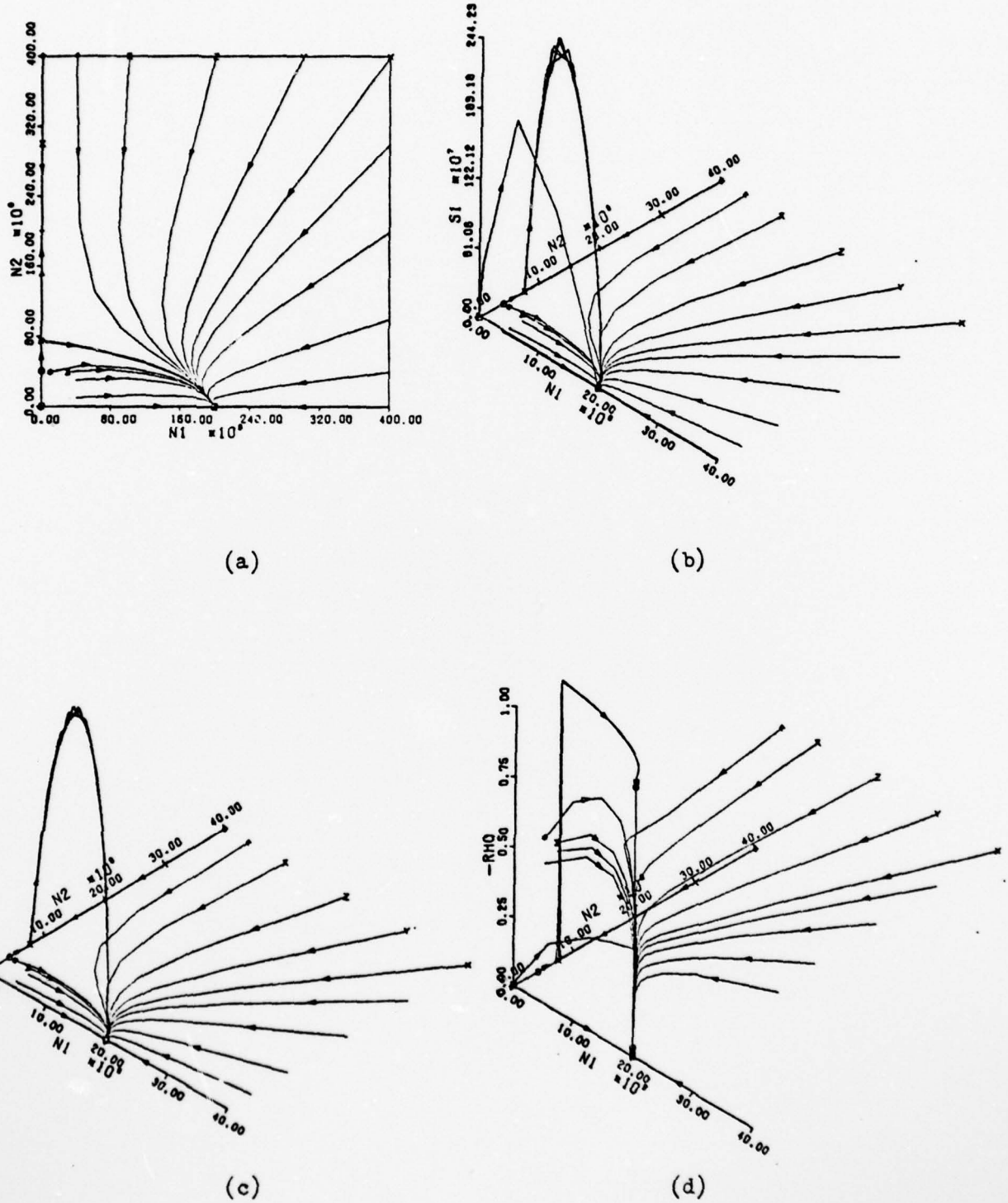

(a) (b)

(c) (d)

Figure 16. Evolution Curves for Case A12

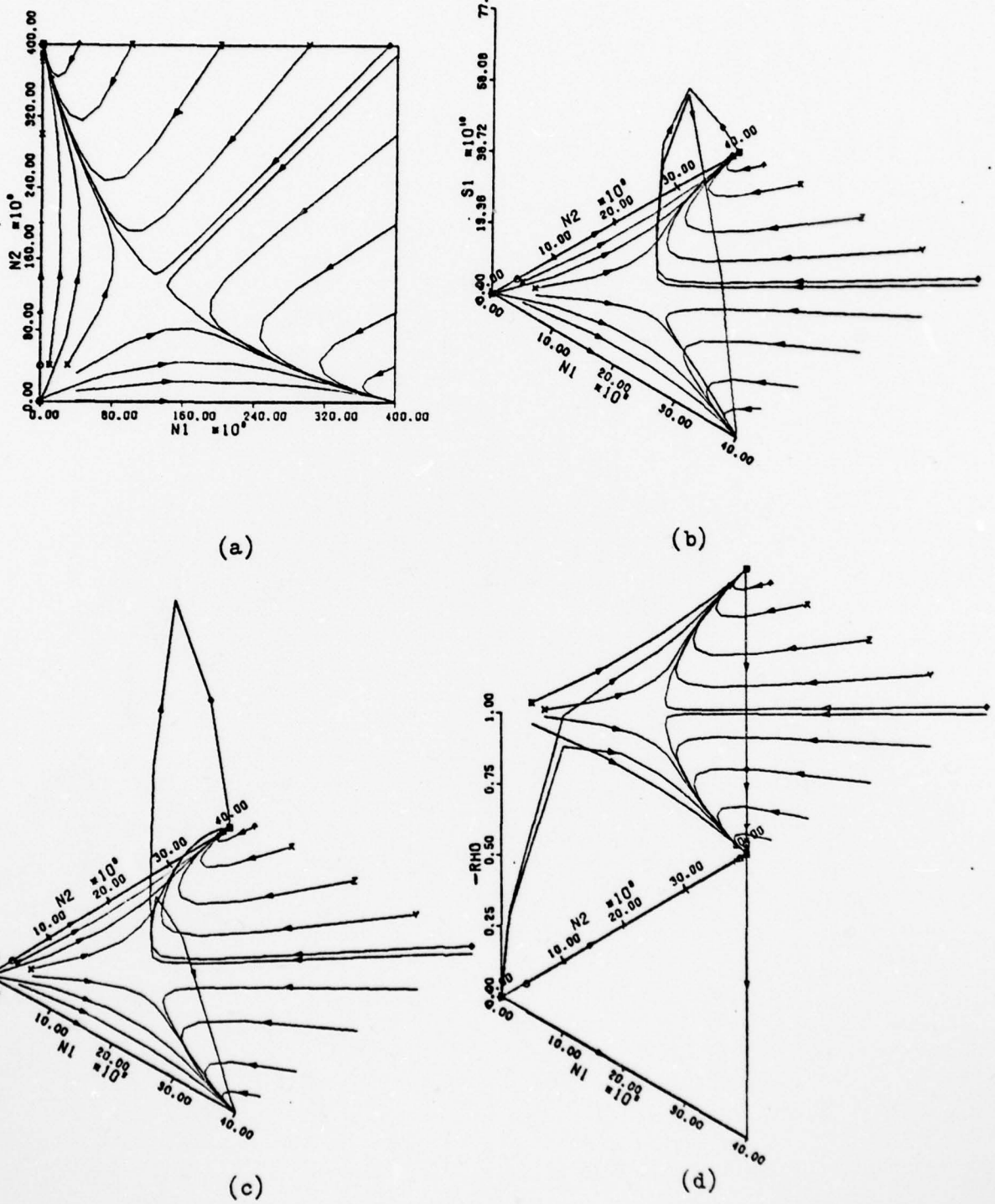

Figure 17. Evolution Curves for Case A13

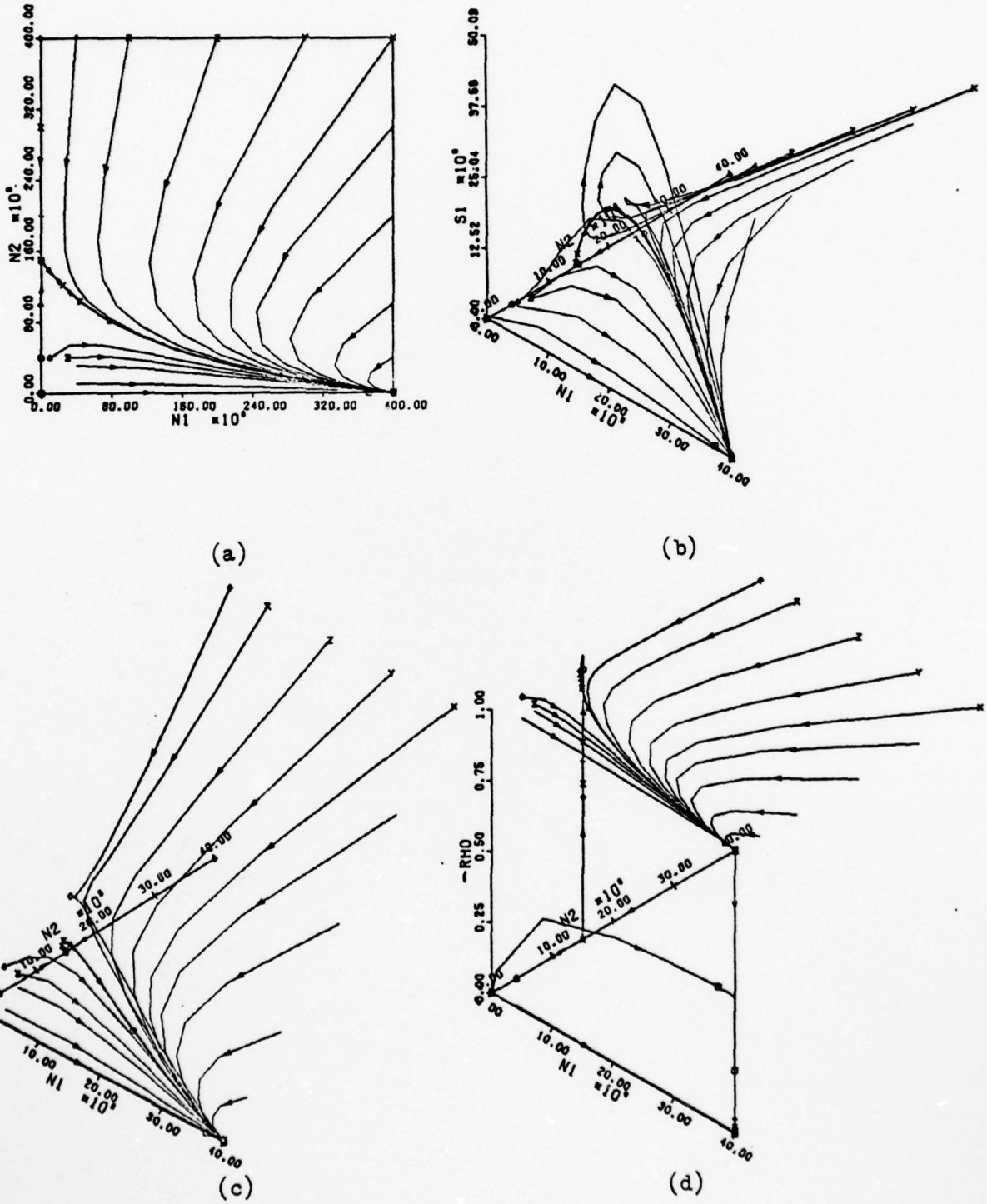

Figure 18. Evolution Curves for Case A14

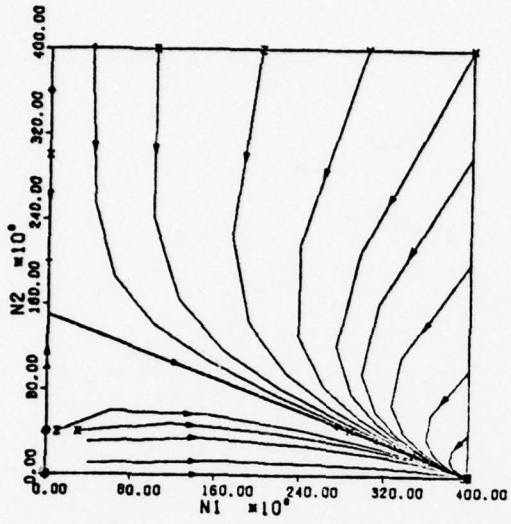

(a)

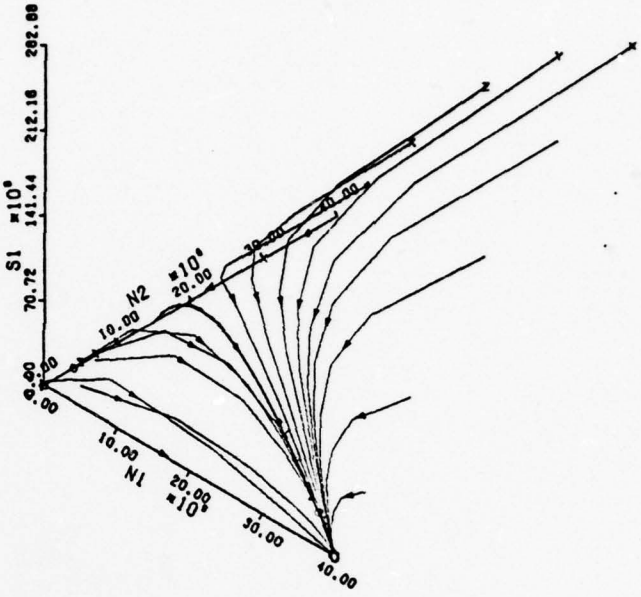

(b)

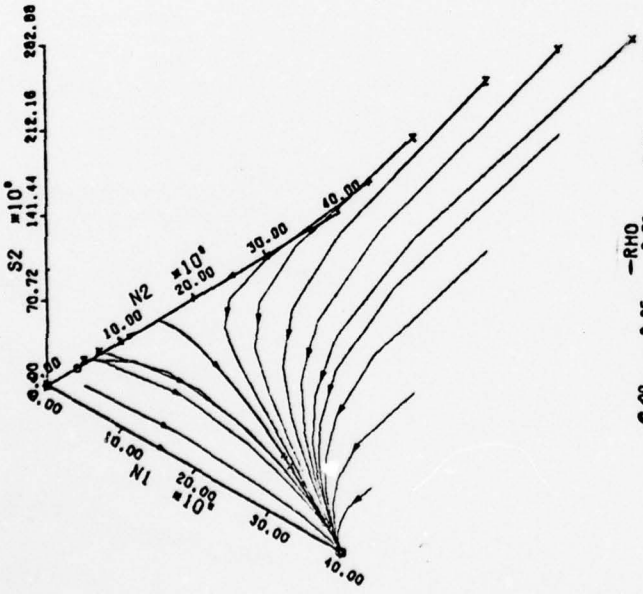

(c)

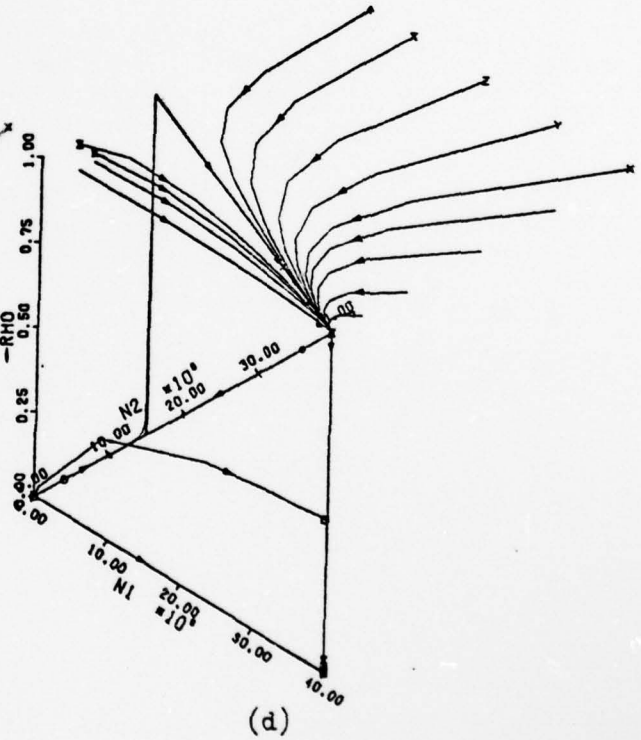

(d)

Figure 19. Evolution Curves for Case A15

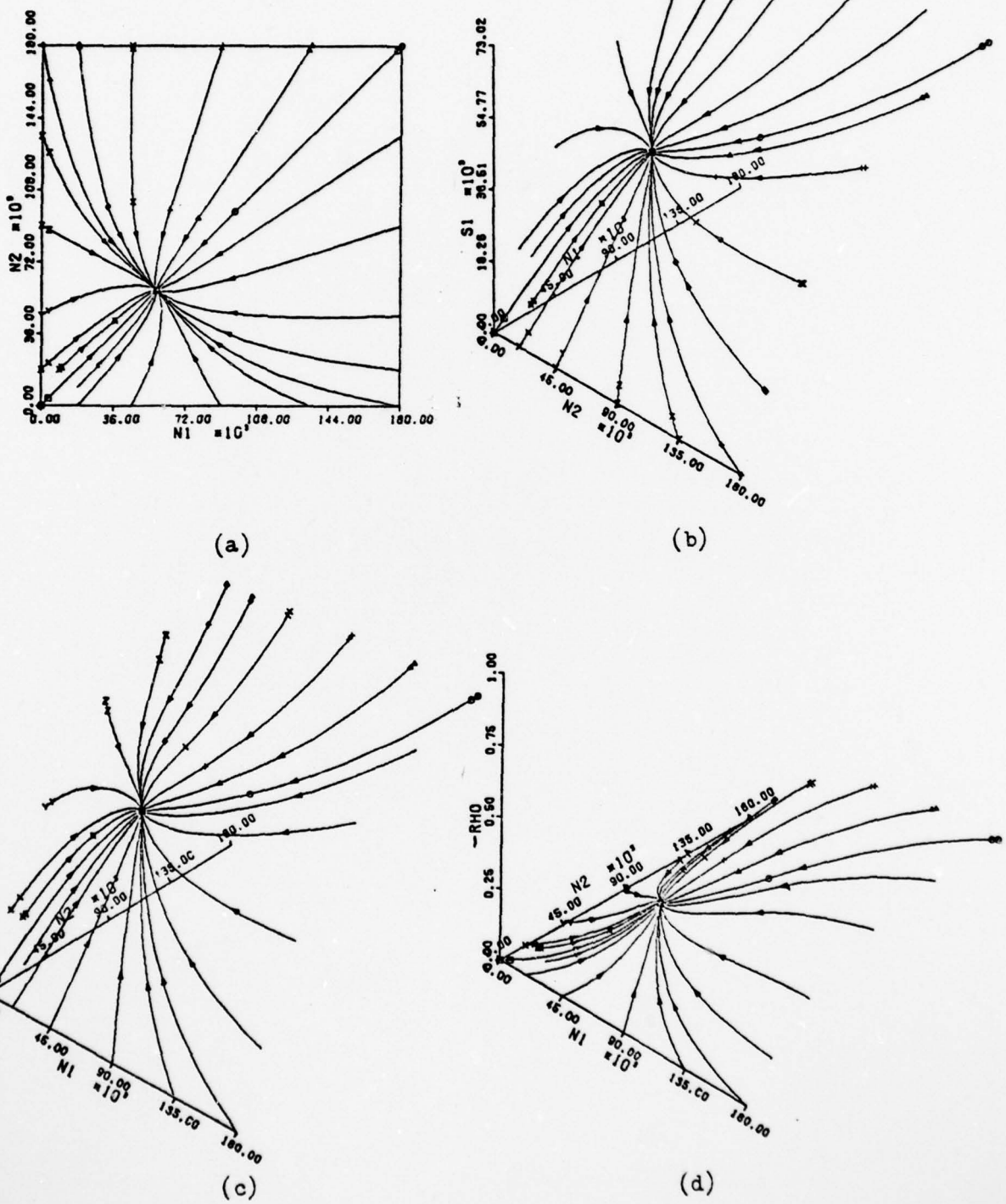

Figure 20. Evolution Curves for Case A31

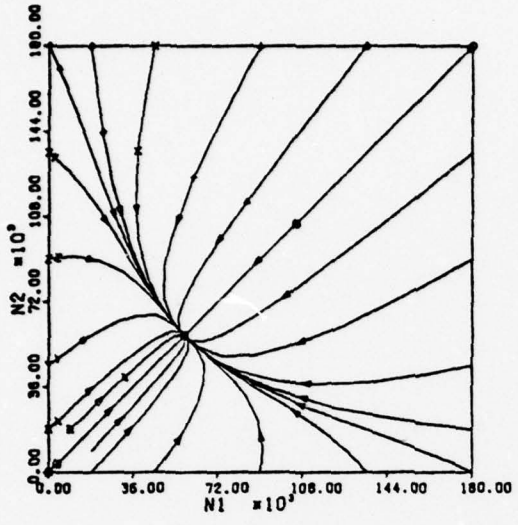

(a)

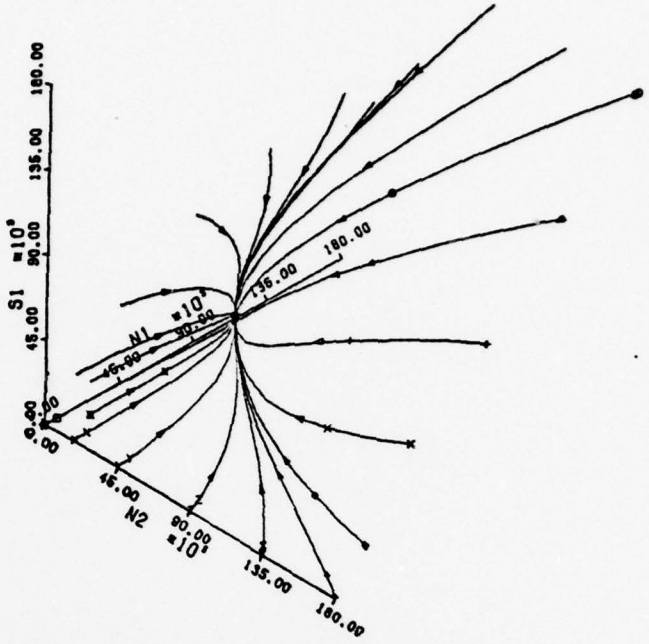

(b)

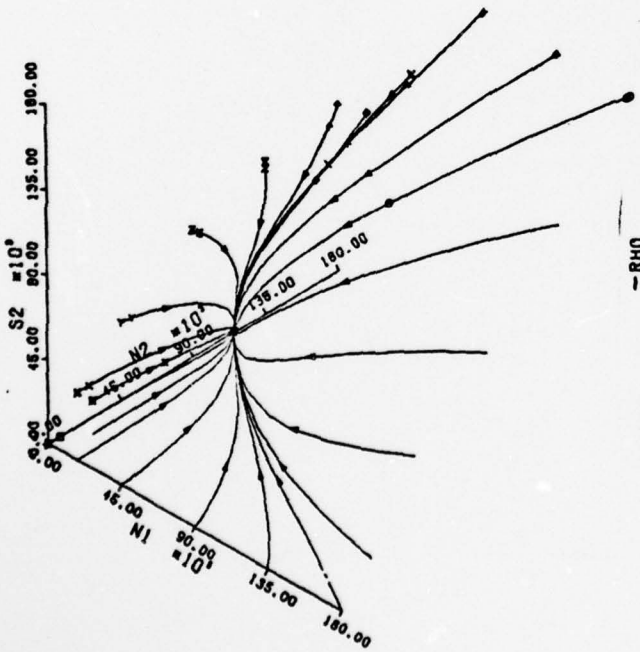

(c)

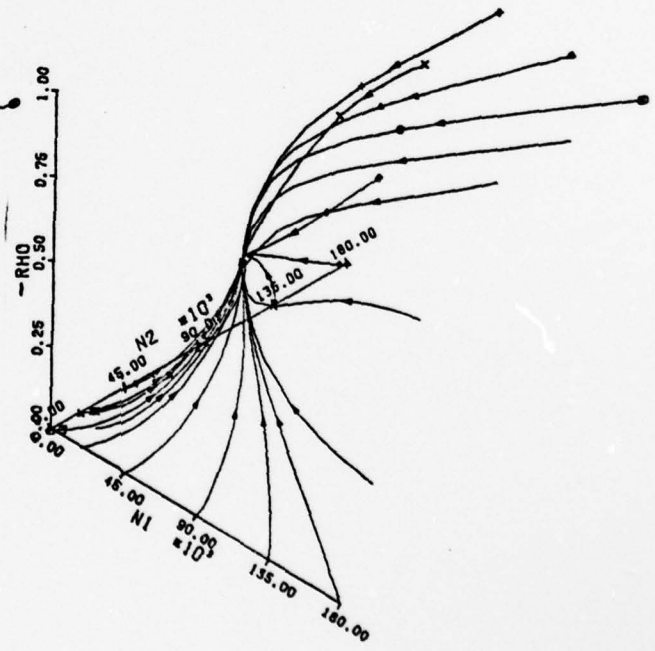

(d)

Figure 21. Evolution Curves for Case A33

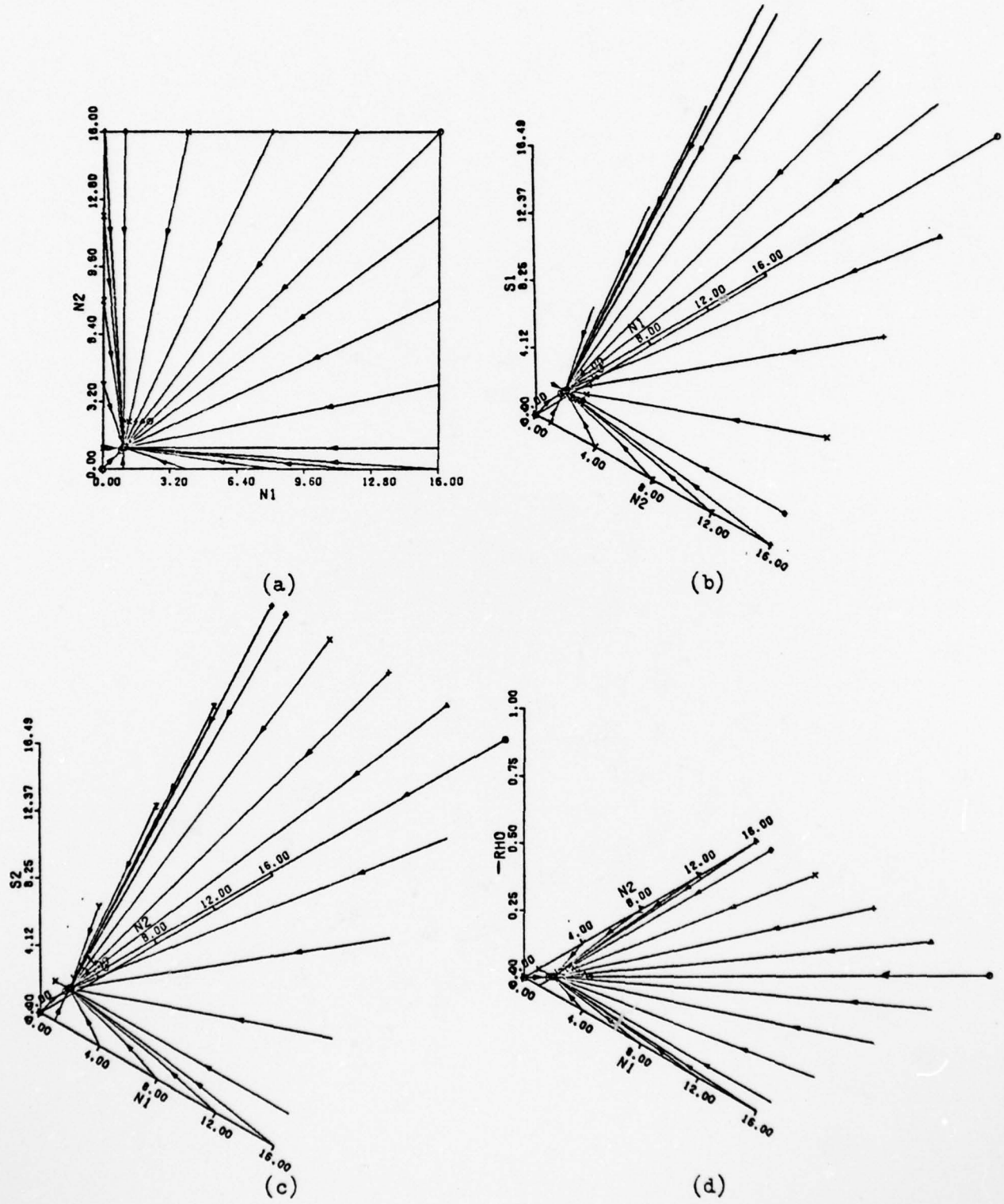

Figure 22. Evolution Curves for Case A51

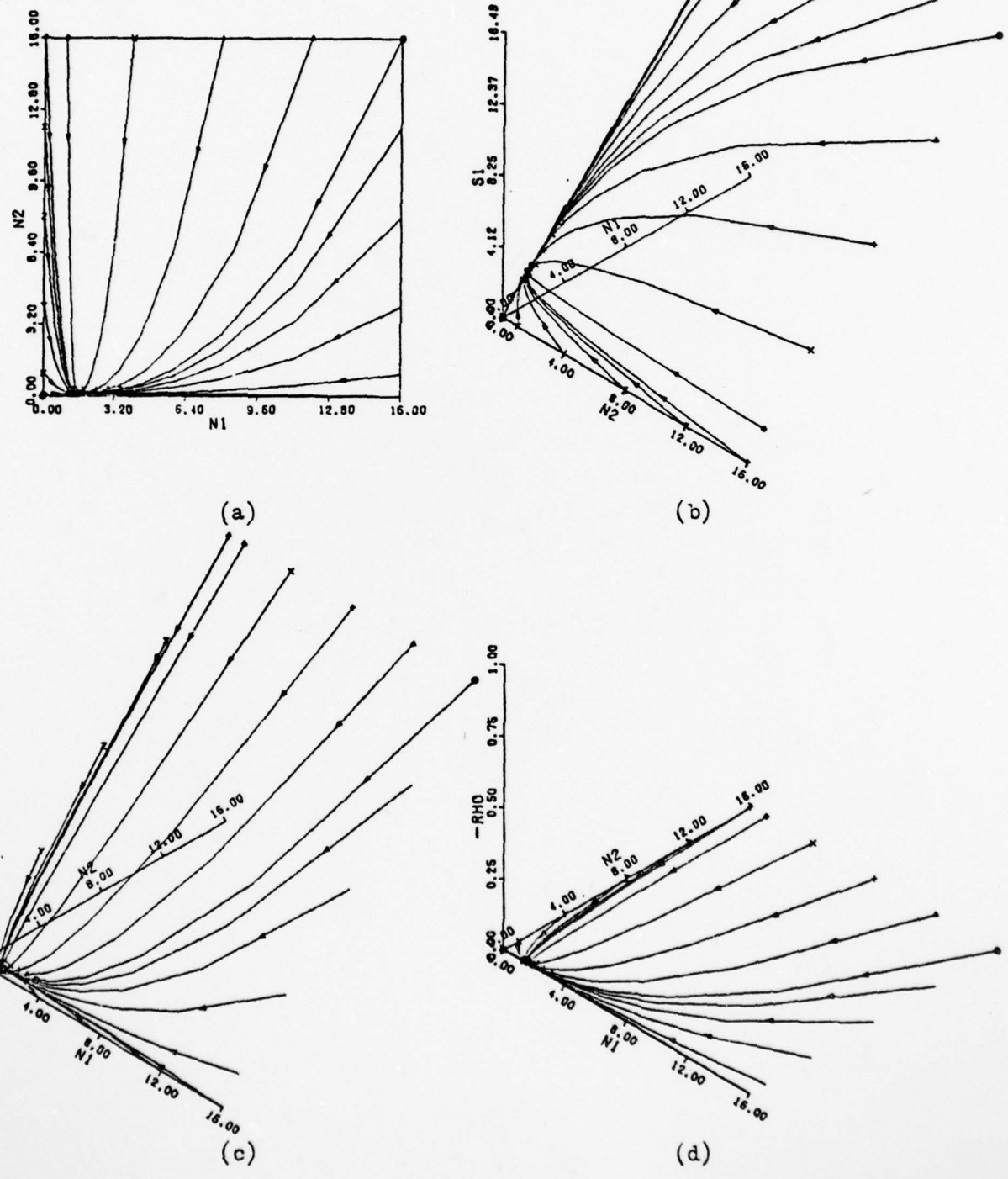

Figure 23. Evolution Curves for Case A52

VITA

Bruce Robert Anderson wa born 16 October 1952 in Salt Lake City, Utah. He graduated from high school in Tustin, California in 1970 and attended the United States Air Force Academy where he majored in physics and mathematics. Upon graduation with distinction he received a Bachelor of Science degree and a commission in the United States Air Force. His initial assignment took him to San Antonio, Texas where he worked as a research physicist for the Laser Effects Branch, School of Aerospace Medicine, Brooks AFB until entering the School of Engineering, Air Force Institute of Technology, in June 1977.

Permanent address: 14128 Cameron Lane
Santa Ana, California 92705

UNCLASSIFIED

SECURITY CLASSIFICATION OF THIS PAGE (When Data Entered)

REPORT DOCUMENTATION PAGE	READ INSTRUCTIONS BEFORE COMPLETING FORM
1. REPORT NUMBER: AFIT/GEP/PH/78-1	2. GOVT ACCESSION NO. / 3. RECIPIENT'S CATALOG NUMBER
4. TITLE (and Subtitle): PHOTON STATISTICS IN TWO-MODE LASERS	5. TYPE OF REPORT & PERIOD COVERED: MS Thesis
	6. PERFORMING ORG. REPORT NUMBER
7. AUTHOR(s): Bruce R. Anderson, Capt USAF	8. CONTRACT OR GRANT NUMBER(s)
9. PERFORMING ORGANIZATION NAME AND ADDRESS: Air Force Institute of Technology (AFIT-EN), Wright-Patterson AFB, Ohio 45433	10. PROGRAM ELEMENT, PROJECT, TASK AREA & WORK UNIT NUMBERS
11. CONTROLLING OFFICE NAME AND ADDRESS	12. REPORT DATE: December 1978
	13. NUMBER OF PAGES: 96
14. MONITORING AGENCY NAME & ADDRESS(if different from Controlling Office)	15. SECURITY CLASS. (of this report): Unclassified
	15a. DECLASSIFICATION/DOWNGRADING SCHEDULE

16. DISTRIBUTION STATEMENT (of this Report)

Approved for public release; distribution unlimited

17. DISTRIBUTION STATEMENT (of the abstract entered in Block 20, if different from Report)

18. SUPPLEMENTARY NOTES

Approved for public release; IAW AFR 190-17

JOSEPH P. HIPPS, MAJOR, USAF
Director of Information 1-23-79

19. KEY WORDS (Continue on reverse side if necessary and identify by block number)

Lasers
Photons
Photon Statistics
Statistics

20. ABSTRACT (Continue on reverse side if necessary and identify by block number)

The evolution of the first and second moments of the photon density distribution for a two-mode laser system was studied by proposing appropriate transition rate expressions and using the Kubo equations developed for a Chapman-Kolmogorov system. A numerical analysis technique was used in solving the rate equations and computer plots were generated for various combinations of laser parameter values. Anomalously large fluctuations, similar to those occurring in single-mode lasers, were observed during →

DD FORM 1 JAN 73 1473 EDITION OF 1 NOV 65 IS OBSOLETE

UNCLASSIFIED

SECURITY CLASSIFICATION OF THIS PAGE (When Data Entered)

AD-A064 394 AIR FORCE INST OF TECH WRIGHT-PATTERSON AFB OHIO SCH--ETC F/G 20/5
PHOTON STATISTICS IN TWO-MODE LASERS.(U)
DEC 78 B R ANDERSON

UNCLASSIFIED AFIT/GEP/PH/78-1 NL

2 OF 2
AD
A064394

END
DATE
FILMED
4-79
DDC

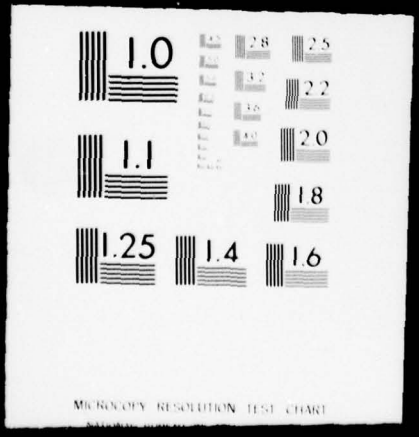

UNCLASSIFIED

SECURITY CLASSIFICATION C

photon buildup o
buildup in the n
lasing mode. In
linear relations

photon buildup of the modes. When only one mode was oscillating, a photon buildup in the non-lasing mode was seen to cause similar fluctuations in the lasing mode. In all cases, these fluctuations were accompanied by a strong linear relationship between the modes.